



CERN-EP-2023-255
13 November 2023

Measurement of (anti)alpha production in central Pb–Pb collisions at $\sqrt{s_{NN}} = 5.02$ TeV

ALICE Collaboration*

Abstract

In this letter, measurements of (anti)alpha production in central (0–10%) Pb–Pb collisions at a center-of-mass energy per nucleon–nucleon pair of $\sqrt{s_{NN}} = 5.02$ TeV are presented, including the first measurement of an antialpha transverse-momentum spectrum. Owing to its large mass, (anti)alpha production yields and transverse-momentum spectra are of particular interest because they provide a stringent test of particle production models. The averaged antialpha and alpha spectrum is included into a common blast-wave fit with lighter particles, indicating that the (anti)alpha also participates in the collective expansion of the medium created in the collision. A blast-wave fit including only protons, (anti)alpha, and other light nuclei results in a similar flow velocity as the fit that includes all particles. A similar flow velocity, but a significantly larger kinetic freeze-out temperature is obtained when only protons and light nuclei are included in the fit. The coalescence parameter B_4 is well described by calculations from a statistical hadronization model but significantly underestimated by calculations assuming nucleus formation via coalescence of nucleons. Similarly, the (anti)alpha-to-proton ratio is well described by the statistical hadronization model. On the other hand, coalescence calculations including approaches with different implementations of the (anti)alpha substructure tend to underestimate the data.

arXiv:2311.11758v1 [nucl-ex] 20 Nov 2023

© 2023 CERN for the benefit of the ALICE Collaboration.

Reproduction of this article or parts of it is allowed as specified in the CC-BY-4.0 license.

*See Appendix A for the list of collaboration members

1 Introduction

During the past five decades the production of light nuclei in heavy-ion reactions has been measured over a broad range of collision energies [1–19]. At center-of-mass energies of up to a few GeV light nucleus production is commonly understood in terms of nuclear break-up where the incoming nuclei disintegrate into lighter nuclear fragments. In contrast to this, the study of the production of antinuclei in heavy-ion collisions is a nascent field that emerged with the availability of heavy-ion colliders [20–36]. In particular, the antialpha was first observed only 13 years ago by the STAR Collaboration in Au–Au collisions at the Relativistic Heavy-Ion Collider (RHIC) [37]. At the Large Hadron Collider (LHC), which provides the highest center-of-mass energies for heavy-ion collisions to date, measurements of the production of nuclei and antinuclei have so far mainly been performed by the ALICE Collaboration in different collision systems [38–55]. Understanding the production mechanism of nuclei and antinuclei in ultrarelativistic collisions could provide deeper insights into the hadronization process and the quantum properties of composite hadronic systems, but a conclusive explanation has yet to be found.

Two different approaches exist that describe the production of light (anti)nuclei in heavy-ion collisions. In statistical hadronization models (SHMs), often simply called thermal models, the production of hadrons and nuclei is described in the framework of a grand-canonical ensemble employing only three parameters: temperature T , volume V , and baryo-chemical potential μ_B [56–62]. Previous measurements of the production of light (anti)nuclei in central Pb–Pb collisions by the ALICE Collaboration agreed well with a common SHM fit to all available hadron and nucleus measurements with a temperature of $T = (156.5 \pm 1.5)$ MeV and a baryo-chemical potential of $\mu_B = (0.7 \pm 3.8)$ MeV [60]. The temperature is commonly understood in terms of a chemical freeze-out temperature T_{ch} at which the abundances of hadrons and nuclei are fixed during the fireball evolution [51, 59]. It is compatible with the (pseudo)critical temperature T_c predicted by the lattice QCD calculations for the transition between a hadronic system and a quark–gluon plasma (QGP) at vanishing μ_B [63, 64]. The interpretation in the context of the production of nuclei, however, is not straightforward because significant modifications of the abundances of nuclei are expected from density and cross-section arguments due to inelastic processes in the subsequent fireball evolution, often called hadronic phase, below T_{ch} .

In another class of models, nucleus formation is conjectured via the coalescence of nucleons in the final state of the system evolution [65–68]. The coalescence process is typically associated with the kinetic freeze-out temperature T_{kin} , which corresponds to the temperature where the inelastic collisions cease and the (transverse) momentum spectra of the particles are frozen [59]. The invariant yield $E_A \frac{d^3 N_A}{d p_A^3}$ of nuclei with mass number A is connected to the final-state momentum distribution of protons $E_p \frac{d^3 N_p}{d p_p^3}$ via the coalescence parameter [67]:

$$B_A = E_A \frac{d^3 N_A}{d p_A^3} \left(E_p \frac{d^3 N_p}{d p_p^3} \right)^{-A}, \quad (1)$$

assuming that protons and neutrons are produced in equal amounts at ultrarelativistic collision energies since both belong to the same isospin doublet. The coalescence prescription can thus be employed to deduce the formation of nuclei based on measured proton yields as well as on nucleon distributions from event generators such as PYTHIA [69, 70] and EPOS [71], or transport models like UrQMD [72–74] or SMASH [75–77].

In pertinent formulations of the coalescence model, the coalescence probability incorporates a dependence on the spatial distribution of the nucleons at kinetic freeze-out and its overlap with the internal wave function of the nuclear cluster, leading to a characteristic dependence of B_A and consequently the production yield of nuclei on the size of the collision system [78–88]. This motivated detailed studies

of nuclear formation in pp, p–Pb, and non-central Pb–Pb collisions, where the yield ratio of nucleus A relative to protons is studied as a function of the average charged-particle multiplicity per unit of pseudorapidity, $\langle dN_{\text{ch}}/d\eta \rangle$. Indeed, the present data tend to confirm the system-size dependence predicted by coalescence models for the yield ratios deuteron to proton (d/p), triton to proton (t/p), and ^3He to proton ($^3\text{He}/\text{p}$) in small collision systems [39, 41–44, 46–48]. On the other hand, the statistical description of particle production in small collision systems requires a canonical formulation of the statistical hadronization model, leading to the Canonical Statistical Model (CSM). This formulation entails an additional model parameter, the so-called correlation volume V_C , inside which electric charge Q , strangeness S , and baryon number B are conserved exactly [61, 62, 89–92]. CSM calculations of nucleus-to-proton ratios result in a suppression of the production of nuclei in small systems that is qualitatively compatible with the patterns observed in data, but still tends to overestimate the yields of nuclei for realistic assumptions of V_C [50, 61, 91].

In central and semi-central Pb–Pb collisions, recent results for d/p and $^3\text{He}/\text{p}$ are compatible with both statistical hadronization and coalescence models, while t/p in Pb–Pb is significantly closer to the coalescence model [52]. It should be noted, however, that the yield of nuclei in Pb–Pb collisions may also be modified by absorption effects during the hadronic phase, as indicated by calculations from the UrQMD model [74].

The observed stiffening of transverse-momentum (p_T) spectra of hadrons produced in heavy-ion collisions can be interpreted in terms of a common radial flow field, arising from hydrodynamic expansion. The so-called blast-wave model [93] describes the radial boost of the light-flavor hadrons and nuclei arising from hydrodynamic expansion with a common set of parameters: the kinetic freeze-out temperature T_{kin} , the mean radial expansion velocity $\langle \beta \rangle$, and an exponent n of the radial velocity profile. The measured p_T spectra are fitted with the Boltzmann-Gibbs blast-wave function [93]:

$$E \frac{d^3N}{dp^3} \propto \int_0^R m_T I_0 \left(\frac{p_T \sinh(\rho(r))}{T_{\text{kin}}} \right) K_1 \left(\frac{m_T \cosh(\rho(r))}{T_{\text{kin}}} \right) r dr \quad (2)$$

where m_T is the transverse mass ($m_T = \sqrt{m^2 + p_T^2}$), I_0 and K_1 are the modified Bessel functions, and ρ is the velocity profile given by:

$$\rho(r) = \tanh^{-1} \beta(r) = \tanh^{-1} \left[\left(\frac{r}{R} \right)^n \beta_{\text{max}} \right], \quad (3)$$

where r is the radial distance in the transverse plane, R is the radius of the fireball and β_{max} is the transverse expansion velocity at the surface of the expanding fireball.

The study of (anti)alpha production in central Pb–Pb collisions is particularly interesting because it is the heaviest nucleus measured at the LHC so far. In the SHM, there is a strong mass dependence of the statistical penalty factor for typical values of T_{ch} and μ_B , while predictions of coalescence models depend on nucleon densities and geometrical factors to the power of A . This makes the (anti)alpha a very sensitive probe for stringent tests of the production models of light nuclei. Previous measurements of the integrated yields of antialpha and alpha in central Pb–Pb collisions at a center-of-mass energy per nucleon–nucleon pair of $\sqrt{s_{\text{NN}}} = 2.76$ TeV agreed with a global fit of the SHM to the yields of all measured hadrons and nuclei [40]. No predictions for $A = 4$ from coalescence models existed at the time.

In this letter, we present results on (anti)alpha production in central Pb–Pb collisions at $\sqrt{s_{\text{NN}}} = 5.02$ TeV, including the first ever measured transverse-momentum spectrum of the antialpha. The results are compared to predictions by coalescence and statistical hadronization models. Together with previous results for different hadron species and lighter nuclei, the p_T spectra are analyzed employing the blast-wave

model. Throughout this letter, especially in the figures but also at some occasions in the text, ${}^4\text{He}$ instead of alpha is stated, which are used as equivalent. Note that with ${}^4\text{He}$ not the chemical element with electron shell but the ${}^4\text{He}$ nucleus is meant.

In Sec. 2 the analysis is described, followed by the presentation of the systematic uncertainties in Sec. 3. The results are discussed in Sec. 4 and the conclusion is given in Sec. 5.

2 Data analysis

The presented results are based on a data set of Pb–Pb collisions at $\sqrt{s_{\text{NN}}} = 5.02$ TeV, collected in 2018, where 99.5×10^6 events in the 0–10% centrality interval [94] were analyzed.

The ALICE apparatus [95, 96] provides excellent particle identification and vertexing capabilities. The (anti)alpha was reconstructed and identified using the Inner Tracking System (ITS), the Time Projection Chamber (TPC), the Transition Radiation Detector (TRD), and the Time-Of-Flight detector (TOF). These detectors are all located inside a homogeneous magnetic field with a strength of 0.5 T and cover the full azimuth in the pseudorapidity range $|\eta| < 0.9$. Interactions located inside $|z| < 10$ cm are selected, where z is the distance from the nominal interaction point along the beam direction.

The ITS [97] is a silicon detector consisting of six cylindrical layers. It is used for charged-particle tracking and for the reconstruction of primary and secondary vertices. It can also be used to separate primary nuclei from secondary, knocked-out nuclei from the detector material, via the distance of closest approach (DCA) of the track to the primary vertex.

The TPC [98] is the main tracking device of the ALICE apparatus. It is a gas-filled cylinder and provides charged-particle tracking and particle identification via the specific energy loss per path length (dE/dx) with a resolution of 6% in Pb–Pb collisions.

The TOF detector [99] provides identification of light (anti)nuclei by means of the velocity determination from the calculated path length of the track and the time-of-flight measurement. Its total time resolution for tracks in Pb–Pb collisions corresponds to about 65 ps which is determined by the intrinsic time resolution of the detector and the resolution of the event collision time measurement. By combining TPC and TOF information, (anti)alphas can be identified from $p_{\text{T}} = 2$ GeV/ c up to 6 GeV/ c in Pb–Pb collisions.

The TRD [100] can be used to improve the momentum resolution and significantly reduces the probability of random matches between tracks and TOF hits.

The V0 detectors [101] measure the arrival time of particles with a resolution of 1 ns, by utilizing a pair of forward and backward scintillator arrays (covering the pseudorapidity ranges $2.8 < \eta < 5.1$ and $-3.7 < \eta < -1.7$). They are used for triggering purposes and for rejection of beam–gas interactions. In addition, they provide the centrality trigger in Pb–Pb collisions [94], and they are also used for offline centrality determination.

The Zero Degree Calorimeter (ZDC) consists of two sets of hadronic calorimeters, which are located 112.5 m away from the interaction point on both sides of it, and of one set of electromagnetic calorimeters, placed 7 m away from the interaction point [95] on one side of it. It is located at 0° relative to the beam direction.

2.1 Event and track selection

The data were collected using a minimum-bias trigger requiring at least one hit in both V0 detectors. Furthermore, a trigger on central collisions was used, also determined by the V0 detectors, selecting collisions in the 0–10% centrality interval. To reject the events triggered by the interactions of the beam with the residual gas in the LHC vacuum pipe, the timing information of the V0 scintillator arrays is

used. A further selection using the ZDC is applied in order to reject the electromagnetic beam–beam interactions and beam–satellite bunch collisions [102]. This is done by selecting good events from the correlation between the sum and the difference of arrival times measured in each of the ZDCs [96]. All these rejection steps are done in the offline analysis.

The production yield of (anti)alphas is measured at midrapidity ($|y| < 0.5$). Only tracks in the full tracking acceptance of $|\eta| < 0.8$ are selected. In order to guarantee good track momentum and dE/dx resolution in the relevant p_T ranges, the selected tracks are required to have at least 70 out of 159 possible reconstructed points in the TPC and at least two points in the ITS out of which at least one is in the two innermost layers, the Silicon Pixel Detector (SPD). The requirement of at least one point in the SPD assures a resolution better than $300 \mu\text{m}$ on the distance of closest approach to the primary vertex for the selected tracks [96]. Furthermore, it is required that the χ^2 per TPC reconstructed point is less than 2.5 and tracks with a kink, which originate from weak decays, where the decay products are one charged and at least one neutral particle, are rejected.

2.2 Particle identification

Particles with electric charge $z = 2$ are well separated in the TPC from the particles with $z = 1$, as they have a four times larger specific energy loss (dE/dx). However, to distinguish the alphas from the much more abundant ${}^3\text{He}$ (by a factor of the order of 10^3) the dE/dx information is combined with the mass calculated from the time-of-flight measured with the TOF and the track momentum. The energy loss in the TPC can be described by the Bethe–Bloch formula for a given mass hypothesis. To select the (anti)alphas it is required that the energy loss of the track lies in a 3σ window around the expected values for alpha particles, where σ is the dE/dx resolution. In addition, it is required that the track is matched to a hit in the TOF detector. Figure 1 shows the m^2/z^2 distribution of the TOF detector for antialpha candidates (green) in the p_T interval between 3 and $6 \text{ GeV}/c$. The m^2/z^2 for true (anti)alphas is $3.475 \text{ GeV}^2/c^4$. Note that in the m^2/z^2 distributions, ${}^4\text{He}$ are clearly separated from ${}^3\text{He}$, for which m^2/z^2 is $2.0 \text{ GeV}^2/c^4$. The background (magenta) is coming from TOF mismatches, which is the case if a track in the TPC is associated with the wrong hit in the TOF detector, resulting in a wrong mass. To describe the background a data-driven approach with only one free parameter is used. The background is determined by selecting all tracks in the TPC outside a 3σ interval of the expected Bethe–Bloch curve for alpha particles and in addition outside a 3σ interval of the expected curve for the deuteron mass hypothesis, as alphas and deuterons have similar m^2/z^2 . The background is then scaled to the height of the ${}^4\text{He}$ histogram by normalizing to the sideband on the right of the ${}^4\text{He}$ peak between 4.4 and $6 \text{ GeV}^2/c^4$ and subtracted. This is done in each p_T interval separately except for the first p_T interval of the ${}^4\overline{\text{He}}$ ($2\text{--}3 \text{ GeV}/c$), where there is no background. The ${}^3\text{He}$ contribution under the ${}^4\text{He}$ peak is described by an exponential fit to the tail of the ${}^3\text{He}$ peak (blue dashed line). This is done in one p_T interval from 3 to $6 \text{ GeV}/c$ and an (anti) ${}^3\text{He}$ fraction (3% for ${}^3\overline{\text{He}}$ and 9% for ${}^3\text{He}$) is determined for particles and antiparticles separately, which is then subtracted in each p_T interval individually. The (anti)alpha signal is counted in every p_T interval between 3 and $4.2 \text{ GeV}^2/c^4$ due to the asymmetric shape of the signal in m^2/z^2 .

The ${}^4\overline{\text{He}}$ raw yield is extracted in four p_T intervals between 2 and $6 \text{ GeV}/c$. The ${}^4\text{He}$ raw yield is only extracted in three p_T intervals between 3 and $6 \text{ GeV}/c$, due to the large contribution of knocked-out alphas from the detector material and the support structure at low p_T . For the statistical uncertainties of the data points the Poisson statistics is used.

2.3 Corrections to the spectra

The transverse-momentum spectra of the (anti)alphas are obtained by correcting the raw yields in the different p_T intervals of the analysis for tracking efficiency and detector acceptance. This is done by using Monte Carlo events, simulated with the HIJING event generator [103]. As HIJING does not include

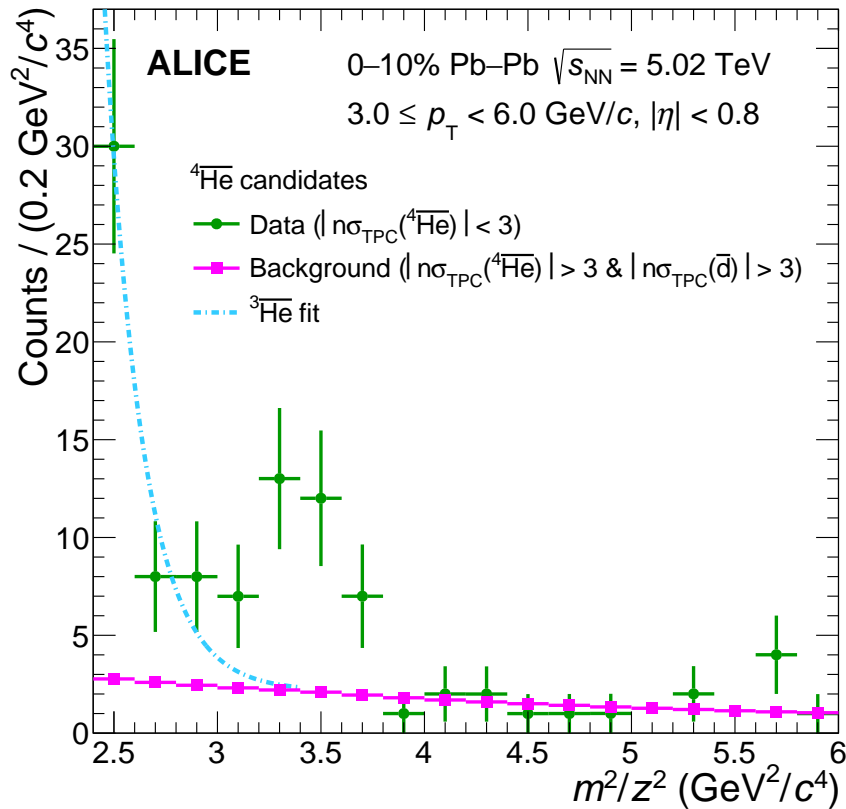


Figure 1: (Color online) m^2/z^2 distribution for ${}^4\overline{\text{He}}$ candidates (green). The background (magenta) is constructed by selecting all candidates outside the ${}^4\overline{\text{He}}$ TPC window of 3σ around the alpha mass hypothesis ($|n\sigma_{\text{TPC}}({}^4\overline{\text{He}})| > 3$) and in addition outside the 3σ window around the deuteron mass hypothesis ($|n\sigma_{\text{TPC}}(\overline{\text{d}})| > 3$). The blue line is an exponential fit to the rise at lower masses originating from ${}^3\overline{\text{He}}$ candidates.

(anti)alphas, they are injected into the event with flat distributions in p_T (between 0 and 10 GeV/c), azimuth (between 0 and 2π), and rapidity ($|y| < 1$). The GEANT4 [104] transport code is used to propagate the generated particles through a full simulation of the ALICE detector setup. The combined acceptance \times efficiency was determined for the (anti)alphas in the 0–10% centrality interval. As the nuclei are not produced with flat p_T distribution, the acceptance \times efficiency was weighted with a blast-wave shape applying an iterative method (see e.g. Ref. [52]), where the blast-wave parameters were taken from a fit to the (anti)alpha spectra.

3 Systematic uncertainties

To estimate the systematic uncertainties, different sources affecting the (anti)alpha measurement were studied, which are described in the following.

The first considered source of systematic uncertainty is related to possible imperfections in the description of the track reconstruction efficiency in the Monte Carlo simulations, which is usually estimated by varying the track selection criteria and by comparing the probability of attaching ITS hits to a TPC track (matching efficiency) in the data and in the simulation. Owing to the low number of counts of the (anti)alpha analysis the systematic variations of the track selection criteria were found to be not significant within the statistical uncertainties by applying the check proposed by Barlow [105]. Therefore, the method based on varying the selections could not be used and instead systematic uncertainties based on similar studies of identified charged particles were assigned, namely 5% for the TPC–ITS matching

efficiency for all p_T intervals [106].

For the signal extraction an uncertainty of 6% was assumed, derived from the analyses of more abundantly produced nuclei, for which a similar method of yield extraction was used [39, 52]. In addition, the scaled background was shifted up and down by 30% and the ${}^3\text{He}$ contribution was determined with different fit ranges of the exponential fit to the tail of the ${}^3\text{He}$ in the m^2/z^2 distribution. This results in an uncertainty for the signal extraction between 6% and 22% for the ${}^4\overline{\text{He}}$ and between 9% and 14% for the ${}^4\text{He}$.

The limited knowledge of the interaction of (anti)nuclei with the detector material leads to another large contribution to the systematic uncertainties. The hadronic interaction cross section implemented in GEANT4 [104, 107–109] is used to determine the acceptance \times efficiency. As there is no measurement of the ${}^4\overline{\text{He}}$ inelastic interaction cross section so far, an uncertainty of 7% is assumed, as done for the ${}^4\overline{\text{He}}$ measured in the Pb–Pb data sample at $\sqrt{s_{\text{NN}}} = 2.76$ TeV [40]. For the alpha an uncertainty for the inelastic cross section of 4% is taken from a measurement of the AMS experiment [110].

The material budget of the ALICE apparatus employed in the MC simulation was varied by $\pm 4.5\%$, corresponding to the uncertainty of the ALICE material budget determination [96]. This results in an uncertainty on the (anti)alpha spectra of 2%.

The blast-wave weighting of the acceptance \times efficiency only affects the first p_T interval of the ${}^4\overline{\text{He}}$ spectrum and the uncertainty was determined to be 3%. This is half of the difference to the case when no blast-wave weighting is taken into account.

As there is a contribution of feed-down to the (anti)alphas from the decay of ${}^4_{\Lambda}\text{H}$ and ${}^4_{\Lambda}\overline{\text{H}}$, an additional uncertainty of 3% for particles and antiparticles in all p_T intervals was taken into account, estimated from a Monte Carlo study where these hypernuclei have been injected.

In total, all these contributions result in a systematic uncertainty between 12% and 24% for ${}^4\overline{\text{He}}$ and between 12% and 16% for ${}^4\text{He}$.

Most of the systematic uncertainties are correlated between ${}^4\text{He}$ and ${}^4\overline{\text{He}}$. The uncorrelated contributions are the uncertainty coming from the inelastic interaction cross section as well as the uncertainties on the background subtraction and the (anti) ${}^3\text{He}$ contribution, which are part of the signal extraction.

4 Results

The size of the data sample presented in this letter exceeds that of a previous measurement in Pb–Pb collisions at $\sqrt{s_{\text{NN}}} = 2.76$ TeV [40] by about a factor of five. This allows for the determination of the transverse-momentum spectra for alpha and antialpha, as shown in Fig. 2. In the case of the antialpha, this is the first ever measurement of the p_T distribution. In the p_T interval between 4 and 5 GeV/ c there is a 2σ discrepancy between particle and antiparticle yields, relative to the combination of statistical and systematic uncertainties, while in the other p_T intervals the alpha and antialpha yields are consistent within statistical uncertainties. The antialpha-to-alpha ratio is shown in the lower panel of Fig. 2, where the error bars represent the statistical uncertainties and the boxes represent the uncorrelated systematic uncertainties, as the correlated ones cancel. Both spectra were combined for further analysis by constructing the weighted average of the data points, where statistical and systematic uncertainties were considered.

The combined (anti)alpha p_T spectrum was compared to those of other light-flavored hadrons [106] and nuclei [52], measured in central (0-10%) Pb–Pb collisions at $\sqrt{s_{\text{NN}}} = 5.02$ TeV, by performing a simultaneous blast-wave fit to all p_T spectra (see Fig. 3, left). The fit range of π , K, p was restricted in the momentum range in order to minimize biases from resonance decays at low p_T and from hard processes at high p_T . The fit is performed in the following p_T intervals: 0.5–1 GeV/ c for charged pions,

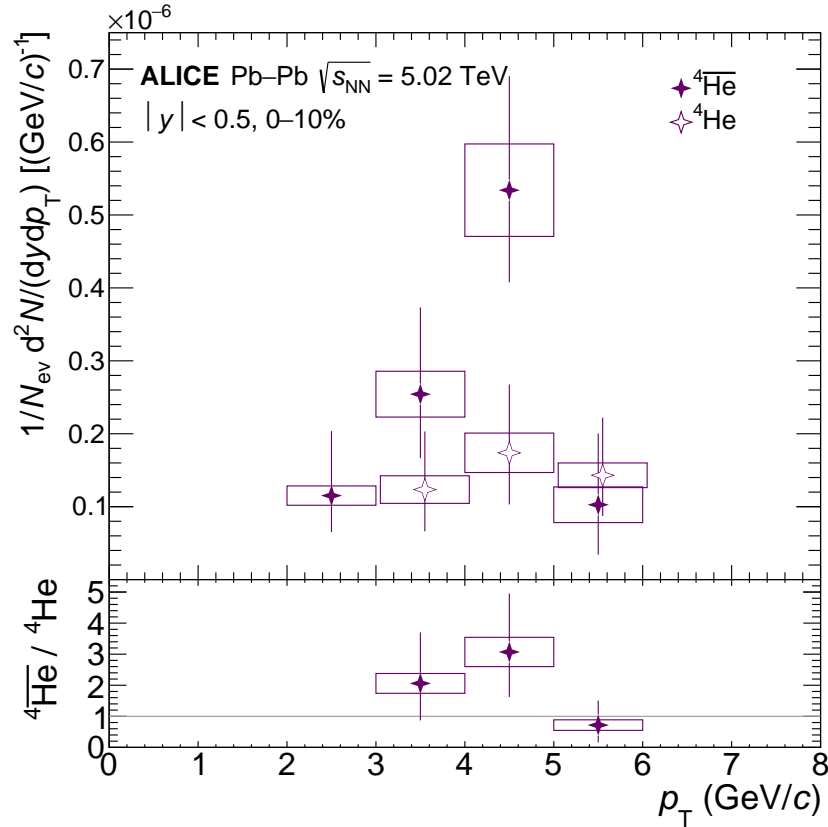


Figure 2: Measured transverse momentum distributions of ${}^4\overline{\text{He}}$ and ${}^4\text{He}$ (upper panel). The vertical lines indicate the statistical uncertainties, while boxes represent the systematic ones. In the case that the statistical uncertainties would overlap the ${}^4\text{He}$ points are a bit shifted on the x-axis. The lower panel shows the ratio between ${}^4\overline{\text{He}}$ and ${}^4\text{He}$ with statistical and uncorrelated systematic uncertainties as the correlated systematic uncertainties cancel.

0.2–1.5 GeV/c for charged kaons, and 0.3–3 GeV/c for (anti)protons. These regions are the same as in the previous publications that showed results for global blast-wave fits [39, 106, 111]. The spectra of antideuterons, antitritons, ${}^3\overline{\text{He}}$, and alpha were fitted over the full measured p_T range.

One should note, blast-wave fits are a simplified approach mimicking the hydrodynamics behind the radial expansion and have certain limitations, e.g. it is known that the temperature is particularly sensitive to the fit range and the used particle species. In particular, in blast-wave fits using the FastReso package [112, 113] the quality of the fits is rather good using a single temperature of about 150 MeV for chemical and kinetic freeze out and these fits do not show a dependence of the temperature on centrality [114]. This is possible in the FastReso approach because the feed-down from resonances is taken into account by the package. In addition, there are other approaches utilizing data from LHC that can describe the data in an extended blast-wave model approach with more parameters [115]. In any case, the standard (Boltzmann-Gibbs) blast-wave fit provides a simple and solid approach to compare the spectra of nuclei and lighter hadrons, which is the goal of the study presented here.

The fit results are shown in the left panel of Fig. 3 and the fit parameters are reported in Table 1 (Fit A). The freeze-out parameters, in particular $\langle\beta\rangle$ and T_{kin} , are consistent with those obtained in Pb–Pb collisions at $\sqrt{s_{NN}} = 2.76$ TeV [39]. The data-to-model ratios, shown in the bottom panel of Fig. 3 left, indicate that the spectra of nuclei are reasonably well described by the common fit within their uncertainties. This suggests that also relatively heavy compound objects like (anti)alpha nuclei participate in a common flow field.

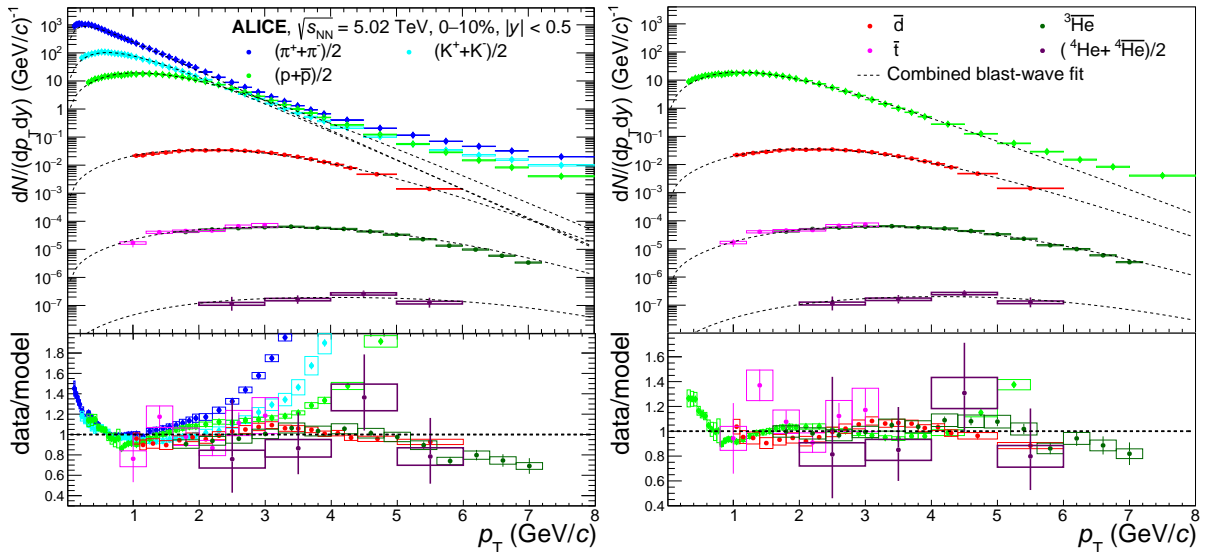


Figure 3: (Color online) Combined blast-wave fit of all available light flavored hadron p_T spectra including nuclei [52, 106] (left) and only p, \bar{d} , \bar{t} , ${}^3\text{He}$ and ${}^4\text{He}$ p_T spectra (right) in Pb–Pb collisions at $\sqrt{s_{NN}} = 5.02$ TeV for 0–10% central events (upper panels). The lower panels show the ratio between each data point and the blast-wave model fit for each species.

Table 1: Parameters obtained from the combined blast-wave fits (Fig. 3) to the p_T spectra of different combinations of light-flavor hadrons and nuclei measured in central (0–10%) Pb–Pb collisions at $\sqrt{s_{NN}} = 5.02$ TeV. The uncertainty from the fits corresponds to the statistical uncertainty. Systematics, that have been evaluated by changing the fit strategy slightly, are of similar size as the statistical uncertainties. The last column shows the χ^2 value and the corresponding number of degrees of freedom (ndf) for each fit.

	Fitted particles	$\langle\beta\rangle$	β_{\max}	T_{kin} (MeV)	n	χ^2 / ndf
Fit A	$\pi, K, p, d, t, {}^3\text{He}, {}^4\text{He}$	0.664 ± 0.002	0.873 ± 0.004	108 ± 2	0.63 ± 0.02	381.1 / 92
Fit B	$p, d, t, {}^3\text{He}, {}^4\text{He}$	0.670 ± 0.002	0.853 ± 0.004	132 ± 4	0.55 ± 0.02	176.5 / 64
Fit C	$d, t, {}^3\text{He}, {}^4\text{He}$	0.684 ± 0.003	0.863 ± 0.005	108 ± 6	0.52 ± 0.02	44.5 / 37
Fit D	π, K, p	0.664 ± 0.002	0.909 ± 0.003	85 ± 4	0.74 ± 0.01	113.0 / 54

The coalescence picture assumes that nuclei are formed at a late stage of the collision, i.e. at or after kinetic freeze-out. In this case, one may expect that the p_T spectra of protons and (anti)nuclei exhibit a common temperature and velocity field that characterizes the source at or after the stage of nuclear cluster formation. To elucidate this further a blast-wave fit was performed, where only protons and (anti)nuclei are included (Fit B). The data points are well described by the common fit, as shown in Fig. 3 (right). Actually, the protons are well described over a larger range in Fit B (right panel of Fig. 3) than in Fit A. The fit parameters indicate a similar velocity field as in the case when π and K are included in the fit (Fit A), but a significantly larger kinetic freeze-out temperature of $T_{\text{kin}} = (132 \pm 4)$ MeV. In the context of final-state coalescence, this finding is unexpected. However, it matches the conjecture of statistical hadronization including formation of (anti)nuclei close to the phase boundary, without significant rescattering at later stages of the system evolution. Possible explanations for such a scenario in terms of pre-hadronic multi-quark states have been proposed in Ref. [60].

The result is challenged by a fit to only the (anti)nuclei (Fit C) which yields $T_{\text{kin}} = (108 \pm 6)$ MeV, which is consistent within the uncertainties with the result of Fit A. This seems to be more in agreement with the expectation of the coalescence model, namely that the protons freeze out earlier as suggested by Fit B, i.e. at a higher temperature, and the nuclei are formed later from these protons and neutrons available for the coalescence process. A fit to only π , K, p (Fit D) results in $T_{\text{kin}} = (85 \pm 4)$ MeV, indicating that

very low apparent kinetic freeze-out temperatures are driven by the lightest particles. It should be noted that lighter particles are more prone to contributions from resonance decays and hard scatterings over a wider p_T range than heavier particles.

From the quality of the fits, i.e. the χ^2/ndf values given in Table 1, it seems like the separation into nuclei (Fit C) and light-flavored hadrons (Fit D) is best. Nevertheless, the temperature of the latter is lower than Fit C, so the coalescence picture is again questioned from this inconsistency between blast-wave results. Indeed, the temperatures extracted from the fits would imply that the protons used in the coalescence process freeze out later than the nuclei formed from them.

Clearly, these findings can not be used for any strong conclusion, in particular since the blast-wave model is only a simplified hydrodynamical picture that has certain limits as discussed above.

The rapidity densities dN/dy are obtained by integration over the blast-wave function. To this end, a blast-wave fit was performed to the p_T spectra of all particles except (anti)alpha. The resulting fit parameters are used to constrain the shape for (anti)alpha while the normalization is obtained by a fit to the (anti)alpha distributions. This procedure was applied separately for the alpha and antialpha p_T distributions as well as to the combined spectrum. The derived rapidity densities are summarized in Table 2. The statistical uncertainties are those of the normalization from the fit, while the systematic uncertainties reflect the variation of dN/dy if the data points are shifted by their systematic uncertainties. The results for alpha and antialpha are consistent within their uncertainties. Also reported are the SHM results obtained from a fit of all available hadron yields using a grand-canonical ensemble [58, 61, 116].

Table 2: Rapidity densities of ${}^4\text{He}$ and ${}^4\overline{\text{He}}$ and their average, together with the statistical hadronization model predictions [58, 61, 116]. The experimental values are giving in addition also the statistical (second value) and systematic uncertainties (third value).

dN/dy (10^{-6}):	${}^4\overline{\text{He}}$	${}^4\text{He}$	$({}^4\overline{\text{He}}+{}^4\text{He})/2$
Experiment	$(1.30 \pm 0.28 \pm 0.18)$	$(0.83 \pm 0.22 \pm 0.12)$	$(1.00 \pm 0.19 \pm 0.10)$
SHM ($T_{\text{ch}} = 156$ MeV)	0.945	0.949	0.947

The presented (anti)alpha transverse-momentum spectra allow for the first time a determination of the coalescence parameter B_4 at LHC energies. To this end, Eq. 1 was employed where the proton p_T distributions were taken from Ref. [106] after averaging the measurements in the 0–5% and 5–10% centrality intervals. The B_4 values shown in Fig. 4 exhibit an increasing trend with p_T/A , which is the transverse momentum per nucleon. This trend is similar to earlier measurements in heavy-ion collisions for lighter nuclei [39, 52]. The results in Fig. 4 are compared to predictions from coalescence [87] and from statistical hadronization models. For the latter, the (anti)alpha and proton yields (dN/dy) are calculated for a chemical freeze-out temperature of $T_{\text{ch}} = 156$ MeV and the shapes of the transverse momentum distributions are taken from the blast-wave fit. While SHM, combined with the spectral shape derived from the blast-wave fit, slightly underpredicts the data, the coalescence prediction is about one order of magnitude below the data in all p_T intervals.

The ratio of alpha to proton dN/dy in central Pb–Pb collisions at $\sqrt{s_{\text{NN}}} = 5.02$ TeV is shown in Fig. 5 as a function of the pseudorapidity density of charged particles produced at midrapidity in the collision, $\langle dN_{\text{ch}}/d\eta \rangle_{|\eta_{\text{lab}}| < 0.5}$. In addition, the ratio from the 10% most central Pb–Pb collisions at $\sqrt{s_{\text{NN}}} = 2.76$ TeV [40] and the upper limit in p–Pb collisions at $\sqrt{s_{\text{NN}}} = 5.02$ TeV [117] are depicted. The new result agrees well with the measurement at lower energy [40]. Furthermore, predictions from the canonical statistical model (CSM) for $T_{\text{ch}} = 155$ MeV and three different values of the correlation volume V_C are displayed [61]. The curves differ at low $\langle dN_{\text{ch}}/d\eta \rangle$, corresponding to the multiplicity of charged particles produced in small collision systems, but coincide in central Pb–Pb collisions where they are consistent within uncertainties with the measurements. Also shown are different calculations from coalescence models. The ‘‘box coalescence’’ (using a maximal difference in coordinate space and momentum for the coalescing partners) implemented in the UrQMD [74] model, indicated by the magenta band (represent-

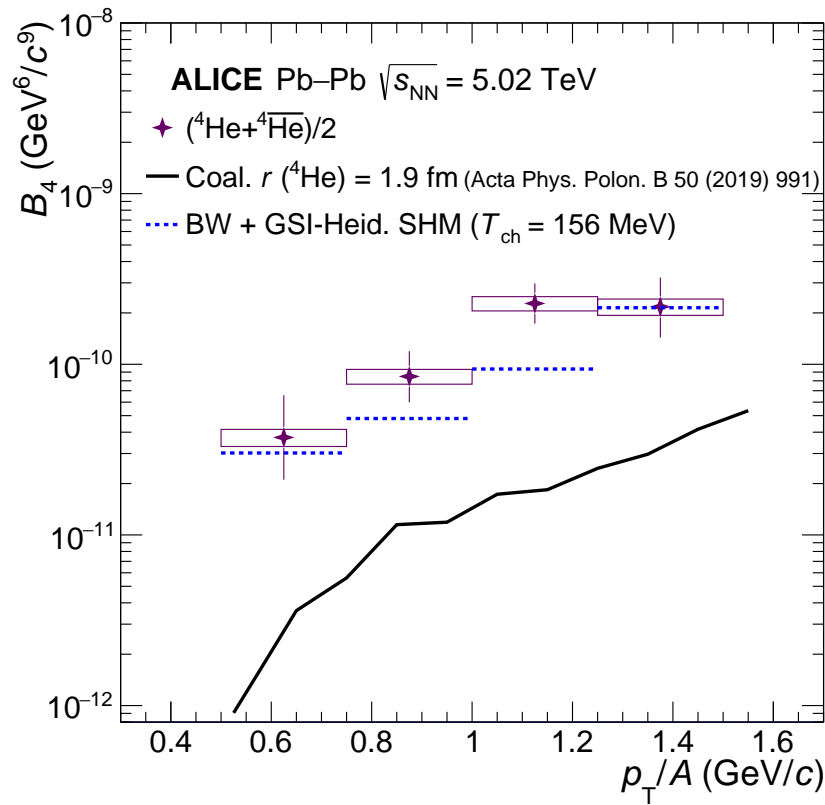


Figure 4: (Color online) The coalescence parameter B_4 as a function of p_T/A , calculated from the averaged ${}^4\text{He}$ and ${}^4\overline{\text{He}}$ spectra and the protons from [106]. Statistical uncertainties are indicated by the vertical lines and the boxes correspond to the systematic uncertainties. The blue dashed line and the full black line indicate the values for the SHM combined with blast-wave p_T shapes and the coalescence predictions from Refs. [86, 87], respectively.

ing the statistical uncertainty of the prediction), shows a non-monotonic behavior that can be explained by absorption processes in the hadronic phase of Pb–Pb collisions [118]. In central Pb–Pb collisions, the UrQMD hybrid model underestimates the data by about a factor of three. Finally, calculations of an analytical coalescence approach are presented, in which the internal structure of the alpha nucleus is taken into account [119]. The assumption of a structureless alpha particle (p-p-n-n) and calculations considering a d-p-n, d-d, ${}^3\text{H-p}$ or ${}^3\text{He-n}$ substructures are compared. All analytical coalescence curves coincide for large system sizes where they underestimate the data by about a factor of three. This might be connected to the fact that the binding energy of the alpha is not taken into account in the model. Neglecting the binding energy might be working well for the $A = 2$ and $A = 3$ nuclei, but not for the alpha, since it is much tighter bound compared to lighter nuclei ($E_B = 2.2$ MeV for the deuteron, whereas the alpha is bound by 28.3 MeV). Interestingly, the presented data even allows for the sum of contributions from coalescence and statistical hadronization predictions. Since these processes are not mutually exclusive one could actually imagine it as interplay of these two production mechanisms.

5 Conclusion

New results on (anti)alpha production in central Pb–Pb collisions at $\sqrt{s_{\text{NN}}} = 5.02$ TeV were presented, including the first differential measurement of the antialpha transverse-momentum distribution. Predictions from statistical hadronization models are compatible with the measured coalescence parameters B_4 and the (anti)alpha-to-proton yield ratio. In contrast, different implementations of the coalescence model underestimate the data significantly. These findings for the production of (anti)alpha are different from

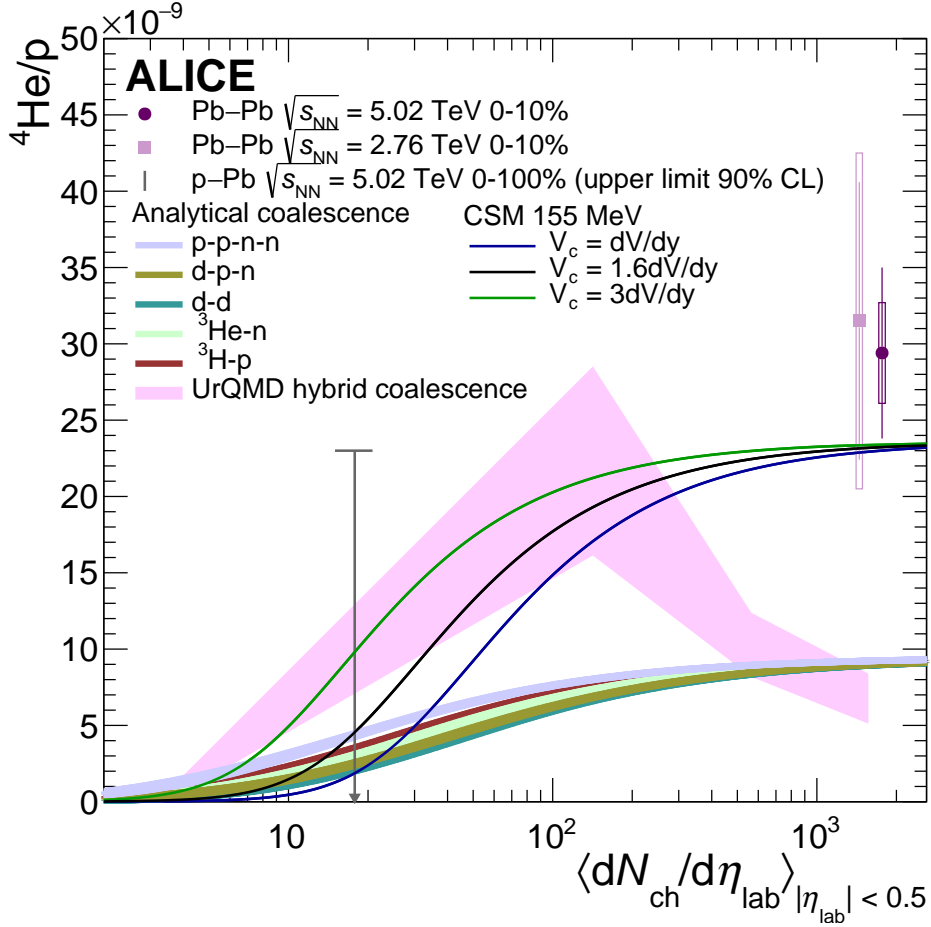


Figure 5: (Color online) ${}^4\text{He}/p$ ratios for the measured data points as a function of charged-particle multiplicity $\langle dN_{ch}/d\eta \rangle_{|\eta_{lab}| < 0.5}$ compared to model predictions. For comparison the result from the 10% most central Pb–Pb collisions at $\sqrt{s_{NN}} = 2.76$ TeV [40] and the upper limit at 90% CL from p–Pb collisions at $\sqrt{s_{NN}} = 5.02$ TeV [117] is also shown. The thermal model curves are from the CSM [61]. For the coalescence model two different approaches are displayed: analytical and UrQMD hybrid coalescence [118, 119]. The analytical coalescence is shown for five different substructures.

the results for $A = 3$ nuclei [52], where both classes of models differ only by about 30% and the data tend to lie in between.

A blast-wave analysis of the p_T distributions together with other hadrons and light nuclei from central Pb–Pb collisions suggests that also relatively heavy compound objects like (anti)alpha nuclei participate in a common flow field. On the other hand, it is remarkable that a blast-wave fit including only protons and light nuclei up to ${}^4\text{He}$ results in a kinetic freeze-out temperature that is rather close to the chemical freeze-out temperature obtained from statistical hadronization models. Note that one should be careful with any strong conclusion from the blast-wave fit, since it has certain limitations. Nevertheless, this result does not agree with naïve expectations based on the coalescence picture, but is in line with a scenario where the yields of light nuclei in central Pb–Pb collisions are dominated by thermal production close to the QCD phase boundary. It should be noted that thermal production and coalescence are not mutually exclusive processes and that the data presented here are even compatible with the sum of contributions from coalescence and statistical hadronization, suggesting a possible interplay of these two production mechanisms.

The recent upgrades of the ALICE detector will enable the collection of substantially larger data samples

during LHC Runs 3 and 4. This will allow for more differential measurements of (anti)alpha production, enabling in particular a systematic study of its dependence on multiplicity and collision system size. The large sensitivity of the (anti)alpha yield to the different production scenarios may help to shed light on the interplay between coalescence and thermal production and a possible transition between them at intermediate system sizes.

Acknowledgements

We thank J. Steinheimer and K.-J. Sun for useful discussions and for providing their predictions.

The ALICE Collaboration would like to thank all its engineers and technicians for their invaluable contributions to the construction of the experiment and the CERN accelerator teams for the outstanding performance of the LHC complex. The ALICE Collaboration gratefully acknowledges the resources and support provided by all Grid centres and the Worldwide LHC Computing Grid (WLCG) collaboration. The ALICE Collaboration acknowledges the following funding agencies for their support in building and running the ALICE detector: A. I. Alikhanyan National Science Laboratory (Yerevan Physics Institute) Foundation (ANSL), State Committee of Science and World Federation of Scientists (WFS), Armenia; Austrian Academy of Sciences, Austrian Science Fund (FWF): [M 2467-N36] and Nationalstiftung für Forschung, Technologie und Entwicklung, Austria; Ministry of Communications and High Technologies, National Nuclear Research Center, Azerbaijan; Conselho Nacional de Desenvolvimento Científico e Tecnológico (CNPq), Financiadora de Estudos e Projetos (Finep), Fundação de Amparo à Pesquisa do Estado de São Paulo (FAPESP) and Universidade Federal do Rio Grande do Sul (UFRGS), Brazil; Bulgarian Ministry of Education and Science, within the National Roadmap for Research Infrastructures 2020-2027 (object CERN), Bulgaria; Ministry of Education of China (MOEC), Ministry of Science & Technology of China (MSTC) and National Natural Science Foundation of China (NSFC), China; Ministry of Science and Education and Croatian Science Foundation, Croatia; Centro de Aplicaciones Tecnológicas y Desarrollo Nuclear (CEADEN), Cubaenergía, Cuba; Ministry of Education, Youth and Sports of the Czech Republic, Czech Republic; The Danish Council for Independent Research | Natural Sciences, the VILLUM FONDEN and Danish National Research Foundation (DNRF), Denmark; Helsinki Institute of Physics (HIP), Finland; Commissariat à l’Energie Atomique (CEA) and Institut National de Physique Nucléaire et de Physique des Particules (IN2P3) and Centre National de la Recherche Scientifique (CNRS), France; Bundesministerium für Bildung und Forschung (BMBF) and GSI Helmholtzzentrum für Schwerionenforschung GmbH, Germany; General Secretariat for Research and Technology, Ministry of Education, Research and Religions, Greece; National Research, Development and Innovation Office, Hungary; Department of Atomic Energy Government of India (DAE), Department of Science and Technology, Government of India (DST), University Grants Commission, Government of India (UGC) and Council of Scientific and Industrial Research (CSIR), India; National Research and Innovation Agency - BRIN, Indonesia; Istituto Nazionale di Fisica Nucleare (INFN), Italy; Japanese Ministry of Education, Culture, Sports, Science and Technology (MEXT) and Japan Society for the Promotion of Science (JSPS) KAKENHI, Japan; Consejo Nacional de Ciencia (CONACYT) y Tecnología, through Fondo de Cooperación Internacional en Ciencia y Tecnología (FONCICYT) and Dirección General de Asuntos del Personal Académico (DGAPA), Mexico; Nederlandse Organisatie voor Wetenschappelijk Onderzoek (NWO), Netherlands; The Research Council of Norway, Norway; Commission on Science and Technology for Sustainable Development in the South (COMSATS), Pakistan; Pontificia Universidad Católica del Perú, Peru; Ministry of Education and Science, National Science Centre and WUT ID-UB, Poland; Korea Institute of Science and Technology Information and National Research Foundation of Korea (NRF), Republic of Korea; Ministry of Education and Scientific Research, Institute of Atomic Physics, Ministry of Research and Innovation and Institute of Atomic Physics and Universitatea Nationala de Stiinta si Tehnologie Politehnica Bucuresti, Romania; Ministry of Education, Science, Research and Sport of the Slovak Republic, Slovakia; National Research Foundation of

South Africa, South Africa; Swedish Research Council (VR) and Knut & Alice Wallenberg Foundation (KAW), Sweden; European Organization for Nuclear Research, Switzerland; Suranaree University of Technology (SUT), National Science and Technology Development Agency (NSTDA) and National Science, Research and Innovation Fund (NSRF via PMU-B B05F650021), Thailand; National Academy of Sciences of Ukraine, Ukraine; Science and Technology Facilities Council (STFC), United Kingdom; National Science Foundation of the United States of America (NSF) and United States Department of Energy, Office of Nuclear Physics (DOE NP), United States of America. In addition, individual groups or members have received support from: European Research Council, Strong 2020 - Horizon 2020 (grant nos. 950692, 824093), European Union; Academy of Finland (Center of Excellence in Quark Matter) (grant nos. 346327, 346328), Finland.

References

- [1] H. H. Gutbrod *et al.*, “Final-state interactions in the production of hydrogen and helium isotopes by relativistic heavy ions on uranium”, *Phys. Rev. Lett.* **37** (1976) 667–670.
- [2] J. Gosset *et al.*, “Central Collisions of Relativistic Heavy Ions”, *Phys. Rev. C* **16** (1977) 629–657.
- [3] S. Nagamiya *et al.*, “Production of pions and light fragments at large angles in high-energy nuclear collisions”, *Phys. Rev. C* **24** (1981) 971–1009.
- [4] S. Nagamiya, J. Randrup, and T. J. M. Symons, “Nuclear collisions at high-energies”, *Ann. Rev. Nucl. Part. Sci.* **34** (1984) 155–187.
- [5] R. L. Auble *et al.*, “Light ion emission from reactions induced by 0.8-2.4 GeV ^{16}O projectiles”, *Phys. Rev. C* **28** (1983) 1552–1564.
- [6] **E886** Collaboration, N. Saito *et al.*, “Composite particle production in relativistic Au+Pt, Si+Pt, and p+Pt collisions”, *Phys. Rev. C* **49** (1994) 3211–3218.
- [7] T. Abbott *et al.*, “Charged hadron distributions in central and peripheral Si + A collisions at 14.6A GeV/c”, *Phys. Rev. C* **50** (1994) 1024–1047.
- [8] **E814** Collaboration, J. Barrette *et al.*, “Production of light nuclei in relativistic heavy-ion collisions”, *Phys. Rev. C* **50** (1994) 1077–1084.
- [9] **EOS** Collaboration, S. Wang *et al.*, “Light fragment production and power law behavior in Au + Au collisions”, *Phys. Rev. Lett.* **74** (1995) 2646–2649.
- [10] **NA44** Collaboration, I. G. Bearden *et al.*, “Deuteron and triton production in Pb + Pb collisions at 158 AGeV”, *Nucl. Phys. A* **661** (1999) 387–390.
- [11] **E864** Collaboration, T. A. Armstrong *et al.*, “Measurements of light nuclei production in 11.5A GeV/c Au+Pb heavy-ion collisions”, *Phys. Rev. C* **61** (2000) 064908, arXiv:nucl-ex/0003009 [nucl-ex].
- [12] **NA49** Collaboration, S. Afanasiev *et al.*, “Deuteron production in central Pb + Pb collisions at 158A GeV”, *Physics Letters B* **486** (2000) 22–28.
- [13] S. Albergo *et al.*, “Light nuclei production in heavy-ion collisions at relativistic energies”, *Phys. Rev. C* **65** (2002) 034907.
- [14] **NA49** Collaboration, T. Anticic *et al.*, “Energy and centrality dependence of deuteron and proton production in Pb+Pb collisions at relativistic energies”, *Phys. Rev. C* **69** (2004) 024902.

- [15] **FOPI** Collaboration, W. Reisdorf *et al.*, “Systematics of central heavy ion collisions in the 1A GeV regime”, *Nucl. Phys. A* **848** (2010) 366–427, arXiv:1005.3418 [nucl-ex].
- [16] **NA49** Collaboration, T. Anticic *et al.*, “Production of deuterium, tritium, and ^3He in central Pb + Pb collisions at 20, 30, 40, 80, and 158 AGeV at the CERN Super Proton Synchrotron”, *Phys. Rev. C* **94** (2016) 044906.
- [17] **HADES** Collaboration, J. Adamczewski-Musch *et al.*, “Directed, Elliptic, and Higher Order Flow Harmonics of Protons, Deuterons, and Tritons in Au+Au Collisions at $\sqrt{s_{\text{NN}}} = 2.4$ GeV”, *Phys. Rev. Lett.* **125** (2020) 262301, arXiv:2005.12217 [nucl-ex].
- [18] **STAR** Collaboration, J. Adam *et al.*, “Beam-energy dependence of the directed flow of deuterons in Au+Au collisions”, *Phys. Rev. C* **102** (2020) 044906, arXiv:2007.04609 [nucl-ex].
- [19] **STAR** Collaboration, M. Abdallah *et al.*, “Light nuclei collectivity from $\sqrt{s_{\text{NN}}} = 3$ GeV Au+Au collisions at RHIC”, *Phys. Lett. B* **827** (2022) 136941, arXiv:2112.04066 [nucl-ex].
- [20] **NA44** Collaboration, J. Simon-Gillo *et al.*, “Deuteron and anti-deuteron production in CERN experiment NA44”, *Nucl. Phys. A* **590** (1995) 483–486.
- [21] **NA44** Collaboration, I. G. Bearden *et al.*, “Anti-deuteron and kaon production in Pb + Pb collisions”, *Nucl. Phys.* **A661** (1999) 55–64.
- [22] **E864** Collaboration, T. A. Armstrong *et al.*, “Antideuteron Yield at the AGS and Coalescence Implications”, *Phys. Rev. Lett.* **85** (2000) 2685–2688, arXiv:nucl-ex/0005001 [nucl-ex].
- [23] M. Aoki *et al.*, “Measurements at 0° of negatively charged particles and antinuclei produced in collisions of 14.6AGeV/c Si on Al, Cu, and Au targets”, *Phys. Rev. Lett.* **69** (1992) 2345–2348.
- [24] **NA49** Collaboration, T. Anticic *et al.*, “Antideuteron and deuteron production in midcentral Pb+Pb collisions at 158AGeV”, *Phys. Rev. C* **85** (2012) 044913.
- [25] **NA52 (NEWMASS)** Collaboration, G. Appelquist *et al.*, “Anti-nuclei production in Pb + Pb collisions at 158 AGeV/c”, *Phys. Lett. B* **376** (1996) 245–250.
- [26] **NA52** Collaboration, M. Weber *et al.*, “The NA52 strangelet and particle search in Pb + Pb collisions at 158 AGeV/c”, *J. Phys. G* **28** (2002) 1921–1927.
- [27] **NA52** Collaboration, G. Ambrosini *et al.*, “Antimatter and matter production in heavy ion collisions at CERN: The NEWMASS experiment NA52”, *Acta Phys. Hung. A* **14** (2001) 297–308, arXiv:nucl-ex/0011016 [nucl-ex].
- [28] **NA52** Collaboration, R. Arsenescu *et al.*, “Anti-helium 3 production in lead-lead collisions at 158 AGeV”, *New J. Phys.* **5** (2003) 1.
- [29] **NA52** Collaboration, R. Arsenescu *et al.*, “An investigation of the antinuclei and nuclei production mechanism in Pb + Pb collisions at 158 AGeV”, *New J. Phys.* **5** (2003) 150.
- [30] **STAR** Collaboration, C. Adler *et al.*, “Antideuteron and anti-helium-3 production in $\sqrt{s_{\text{NN}}} = 130$ GeV Au + Au collisions”, *Phys. Rev. Lett.* **87** (2001) 262301, arXiv:nucl-ex/0108022.
- [31] **PHENIX** Collaboration, S. Afanasiev *et al.*, “Elliptic flow for phi mesons and (anti)deuterons in Au + Au collisions at $\sqrt{s_{\text{NN}}} = 200$ GeV”, *Phys. Rev. Lett.* **99** (2007) 052301, arXiv:nucl-ex/0703024 [NUCL-EX].

- [32] **PHENIX** Collaboration, S. S. Adler *et al.*, “Deuteron and Antideuteron Production in Au+Au Collisions at $\sqrt{s_{NN}} = 200$ GeV”, *Phys. Rev. Lett.* **94** (2005) 122302, arXiv:nucl-ex/0406004 [nucl-ex].
- [33] **BRAHMS** Collaboration, C. Nygaard, “Rapidity dependence of coalescence in Au+Au collisions at $\sqrt{s_{NN}} = 200$ GeV”, *J. Phys. G* **34** (2007) S1065–S1068.
- [34] **STAR** Collaboration, B. Abelev *et al.*, “Yields and elliptic flow of d(anti-d) and He-3(anti-He-3) in Au + Au collisions at $\sqrt{s_{NN}} = 200$ GeV”, arXiv:0909.0566 [nucl-ex].
- [35] **BRAHMS** Collaboration, I. Arsene *et al.*, “Rapidity dependence of deuteron production in Au+Au collisions at $\sqrt{s_{NN}} = 200$ GeV”, *Phys. Rev. C* **83** (2011) 044906, arXiv:1005.5427 [nucl-ex].
- [36] **STAR** Collaboration, J. Adam *et al.*, “Beam energy dependence of (anti-)deuteron production in Au + Au collisions at the BNL Relativistic Heavy Ion Collider”, *Phys. Rev. C* **99** (2019) 064905, arXiv:1903.11778 [nucl-ex].
- [37] **STAR** Collaboration, H. Agakishiev *et al.*, “Observation of the antimatter helium-4 nucleus”, *Nature* **473** (2011) 353, arXiv:1103.3312 [nucl-ex].
- [38] **ALICE** Collaboration, J. Adam *et al.*, “Precision measurement of the mass difference between light nuclei and anti-nuclei”, *Nature Phys.* **11** (2015) 811–814, arXiv:1508.03986 [nucl-ex].
- [39] **ALICE** Collaboration, J. Adam *et al.*, “Production of light nuclei and anti-nuclei in pp and Pb–Pb collisions at energies available at the CERN Large Hadron Collider”, *Phys. Rev. C* **93** (2016) 024917, arXiv:1506.08951 [nucl-ex].
- [40] **ALICE** Collaboration, S. Acharya *et al.*, “Production of ^4He and $^4\overline{\text{He}}$ in Pb–Pb collisions at $\sqrt{s_{NN}} = 2.76$ TeV at the LHC”, *Nucl. Phys. A* **971** (2018) 1–20, arXiv:1710.07531 [nucl-ex].
- [41] **ALICE** Collaboration, S. Acharya *et al.*, “Production of deuterons, tritons, ^3He nuclei and their antinuclei in pp collisions at $\sqrt{s} = 0.9, 2.76$ and 7 TeV”, *Phys. Rev. C* **97** (2018) 024615, arXiv:1709.08522 [nucl-ex].
- [42] **ALICE** Collaboration, S. Acharya *et al.*, “Multiplicity dependence of (anti-)deuteron production in pp collisions at $\sqrt{s} = 7$ TeV”, *Phys. Lett. B* **794** (2019) 50–63, arXiv:1902.09290 [nucl-ex].
- [43] **ALICE** Collaboration, S. Acharya *et al.*, “Multiplicity dependence of light (anti-)nuclei production in p–Pb collisions at $\sqrt{s_{NN}} = 5.02$ TeV”, *Phys. Lett. B* **800** (2020) 135043, arXiv:1906.03136 [nucl-ex].
- [44] **ALICE** Collaboration, S. Acharya *et al.*, “(Anti-)deuteron production in pp collisions at $\sqrt{s} = 13$ TeV”, *Eur. Phys. J. C* **80** (2020) 889, arXiv:2003.03184 [nucl-ex].
- [45] **ALICE** Collaboration, S. Acharya *et al.*, “Measurement of the low-energy antideuteron inelastic cross section”, *Phys. Rev. Lett.* **125** (2020) 162001, arXiv:2005.11122 [nucl-ex].
- [46] **ALICE** Collaboration, S. Acharya *et al.*, “Jet-associated deuteron production in pp collisions at $\sqrt{s} = 13$ TeV”, *Phys. Lett. B* **819** (2021) 136440, arXiv:2011.05898 [nucl-ex].
- [47] **ALICE** Collaboration, S. Acharya *et al.*, “Production of light (anti)nuclei in pp collisions at $\sqrt{s} = 13$ TeV”, *JHEP* **01** (2022) 106, arXiv:2109.13026 [nucl-ex].

- [48] **ALICE** Collaboration, S. Acharya *et al.*, “Production of light (anti)nuclei in pp collisions at $\sqrt{s} = 5.02$ TeV”, *Eur. Phys. J. C* **82** (2022) 289, arXiv:2112.00610 [nucl-ex].
- [49] **ALICE** Collaboration, S. Acharya *et al.*, “Measurement of anti- ^3He nuclei absorption in matter and impact on their propagation in the Galaxy”, *Nature Phys.* **19** (2023) 61–71, arXiv:2202.01549 [nucl-ex].
- [50] **ALICE** Collaboration, S. Acharya *et al.*, “First Measurement of Antideuteron Number Fluctuations at Energies Available at the Large Hadron Collider”, *Phys. Rev. Lett.* **131** (2023) 041901, arXiv:2204.10166 [nucl-ex].
- [51] **ALICE** Collaboration, “The ALICE experiment – A journey through QCD”, arXiv:2211.04384 [nucl-ex].
- [52] **ALICE** Collaboration, S. Acharya *et al.*, “Light (anti)nuclei production in Pb–Pb collisions at $\sqrt{s_{NN}} = 5.02$ TeV”, *Phys. Rev. C* **107** (2023) 064904, arXiv:2211.14015 [nucl-ex].
- [53] **ALICE** Collaboration, S. Acharya *et al.*, “Enhanced Deuteron Coalescence Probability in Jets”, *Phys. Rev. Lett.* **131** (2023) 042301, arXiv:2211.15204 [nucl-ex].
- [54] **ALICE** Collaboration, S. Acharya *et al.*, “Measurement of the production of (anti)nuclei in p–Pb collisions at $s_{NN}=8.16$ TeV”, *Phys. Lett. B* **846** (2023) 137795, arXiv:2212.04777 [nucl-ex].
- [55] **ALICE** Collaboration, S. Acharya *et al.*, “Measurement of the low-energy antitriton inelastic cross section”, arXiv:2307.03603 [nucl-ex].
- [56] P. Braun-Munzinger and J. Stachel, “Production of strange clusters and strange matter in nucleus-nucleus collisions at the AGS”, *J. Phys. G* **21** (1995) L17–L20, arXiv:nucl-th/9412035 [nucl-th].
- [57] P. Braun-Munzinger, K. Redlich, and J. Stachel, *Particle production in heavy ion collisions, invited review in: R.C. Hwa, X.N. Wang Eds., Quark Gluon Plasma, vol. 3.* World Scientific Publishing, 2003. arXiv:nucl-th/0304013.
- [58] A. Andronic *et al.*, “Production of light nuclei, hypernuclei and their antiparticles in relativistic nuclear collisions”, *Phys. Lett. B* **697** (2011) 203–207, arXiv:1010.2995 [nucl-th].
- [59] P. Braun-Munzinger and B. Dönigus, “Loosely-bound objects produced in nuclear collisions at the LHC”, *Nucl. Phys. A* **987** (2019) 144–201, arXiv:1809.04681 [nucl-ex].
- [60] A. Andronic *et al.*, “Decoding the phase structure of QCD via particle production at high energy”, *Nature* **561** (2018) 321–330, arXiv:1710.09425 [nucl-th].
- [61] V. Vovchenko, B. Dönigus and H. Stoecker, “Multiplicity dependence of light nuclei production at LHC energies in the canonical statistical model”, *Phys. Lett. B* **785** (2018) 171–174, arXiv:1808.05245 [hep-ph].
- [62] B. Dönigus, “Light nuclei in the hadron resonance gas”, *Int. J. Mod. Phys. E* **29** (2020) 2040001, arXiv:2004.10544 [nucl-th].
- [63] **HotQCD** Collaboration, A. Bazavov *et al.*, “Chiral crossover in QCD at zero and non-zero chemical potentials”, *Phys. Lett. B* **795** (2019) 15–21, arXiv:1812.08235 [hep-lat].
- [64] S. Borsanyi, Z. Fodor, J. N. Guenther, R. Kara, S. D. Katz, P. Parotto, A. Pasztor, C. Ratti, and K. K. Szabo, “QCD Crossover at Finite Chemical Potential from Lattice Simulations”, *Phys. Rev. Lett.* **125** (2020) 052001, arXiv:2002.02821 [hep-lat].

- [65] S. Butler and C. Pearson, “Deuterons from high-energy proton bombardment of matter”, *Phys. Rev.* **129** (1963) 836–842.
- [66] J. I. Kapusta, “Mechanisms for deuteron production in relativistic nuclear collisions”, *Phys. Rev. C* **21** (1980) 1301–1310.
- [67] L. Csernai and J. I. Kapusta, “Entropy and Cluster Production in Nuclear Collisions”, *Phys. Rept.* **131** (1986) 223–318.
- [68] J. Steinheimer *et al.*, “Hypernuclei, dibaryon and antinuclei production in high energy heavy ion collisions: Thermal production versus Coalescence”, *Phys. Lett. B* **714** (2012) 85–91, arXiv:1203.2547 [nucl-th].
- [69] T. Sjöstrand *et al.*, “An introduction to PYTHIA 8.2”, *Comput. Phys. Commun.* **191** (2015) 159–177, arXiv:1410.3012 [hep-ph].
- [70] C. Bierlich *et al.*, “A comprehensive guide to the physics and usage of PYTHIA 8.3”, arXiv:2203.11601 [hep-ph].
- [71] T. Pierog *et al.*, “EPOS LHC: Test of collective hadronization with data measured at the CERN Large Hadron Collider”, *Phys. Rev. C* **92** (2015) 034906, arXiv:1306.0121 [hep-ph].
- [72] S. Bass *et al.*, “Microscopic models for ultrarelativistic heavy ion collisions”, *Prog.Part.Nucl. Phys.* **41** (1998) 255–369, arXiv:nucl-th/9803035 [nucl-th].
- [73] S. Sombun *et al.*, “Deuteron production from phase-space coalescence in the UrQMD approach”, *Phys. Rev. C* **99** (2019) 014901, arXiv:1805.11509 [nucl-th].
- [74] T. Reichert *et al.*, “Energy dependence of light hypernuclei production in heavy-ion collisions from a coalescence and statistical-thermal model perspective”, *Phys. Rev. C* **107** (2023) 014912, arXiv:2210.11876 [nucl-th].
- [75] D. Oliinychenko, L.-G. Pang, H. Elfner, and V. Koch, “Centrality dependence of deuteron production in Pb+Pb collisions at 2.76 TeV via hydrodynamics and hadronic afterburner”, *MDPI Proc.* **10** (2019) 6, arXiv:1812.06225 [hep-ph].
- [76] D. Oliinychenko, L.-G. Pang, H. Elfner, and V. Koch, “Microscopic study of deuteron production in PbPb collisions at $\sqrt{s} = 2.76$ TeV via hydrodynamics and a hadronic afterburner”, *Phys. Rev. C* **99** (2019) 044907, arXiv:1809.03071 [hep-ph].
- [77] H. Petersen *et al.*, “SMASH – A new hadronic transport approach”, *Nucl. Phys. A* **982** (2019) 399–402, arXiv:1808.06832 [nucl-th].
- [78] S. Mrowczynski, “Deuteron formation mechanism”, *J. Phys. G* **13** (1987) 1089–1097.
- [79] S. Mrowczynski, “Anti-deuteron Production and the Size of the Interaction Zone”, *Phys. Lett. B* **248** (1990) 459–463.
- [80] S. Mrowczynski, “On the neutron proton correlations and deuteron production”, *Phys. Lett. B* **277** (1992) 43–48.
- [81] R. Scheibl and U. W. Heinz, “Coalescence and flow in ultrarelativistic heavy ion collisions”, *Phys. Rev. C* **59** (1999) 1585–1602, arXiv:nucl-th/9809092 [nucl-th].
- [82] K. Blum, R. Sato, and E. Waxman, “Cosmic-ray Antimatter”, arXiv:1709.06507 [astro-ph.HE].

- [83] K.-J. Sun and L.-W. Chen, “Analytical coalescence formula for particle production in relativistic heavy-ion collisions”, *Phys. Rev. C* **95** (2017) 044905, arXiv:1701.01935 [nucl-th].
- [84] K.-J. Sun, C.-M. Ko and B. Dönigus, “Suppression of light nuclei production in collisions of small systems at the Large Hadron Collider”, *Phys. Lett. B* **792** (2019) 132–137, arXiv:1812.05175 [nucl-th].
- [85] K. Blum and M. Takimoto, “Nuclear coalescence from correlation functions”, *Phys. Rev. C* **99** (2019) 044913, arXiv:1901.07088 [nucl-th].
- [86] F. Bellini and A. P. Kalweit, “Testing production scenarios for (anti-)(hyper-)nuclei and exotica at energies available at the CERN Large Hadron Collider”, *Phys. Rev. C* **99** (2019) 054905, arXiv:1807.05894 [hep-ph].
- [87] F. Bellini and A. P. Kalweit, “Testing production scenarios for (anti-)(hyper-)nuclei with multiplicity-dependent measurements at the LHC”, *Acta Phys. Polon. B* **50** (2019) 991, arXiv:1907.06868 [hep-ph].
- [88] F. Bellini, K. Blum, A. P. Kalweit, and M. Puccio, “Examination of coalescence as the origin of nuclei in hadronic collisions”, *Phys. Rev. C* **103** (2021) 014907, arXiv:2007.01750 [nucl-th].
- [89] F. Becattini *et al.*, “Features of particle multiplicities and strangeness production in central heavy ion collisions between 1.7 AGeV/c and 158 AGeV/c”, *Phys. Rev. C* **64** (2001) 024901, arXiv:hep-ph/0002267 [hep-ph].
- [90] N. Sharma, J. Cleymans, B. Hippolyte, and M. Paradza, “A Comparison of p-p, p–Pb, Pb–Pb Collisions in the Thermal Model: Multiplicity Dependence of Thermal Parameters”, *Phys. Rev. C* **99** (2019) 044914, arXiv:1811.00399 [hep-ph].
- [91] V. Vovchenko, B. Dönigus and H. Stoecker, “Canonical statistical model analysis of p-p, p–Pb, and Pb–Pb collisions at energies available at the CERN Large Hadron Collider”, *Phys. Rev. C* **100** (2019) 054906, arXiv:1906.03145 [hep-ph].
- [92] N. Sharma, L. Kumar, P. M. Lo, and K. Redlich, “Light-nuclei production in pp and pA collisions in the baryon canonical ensemble approach”, *Phys. Rev. C* **107** (2023) 054903, arXiv:2210.15617 [nucl-th].
- [93] E. Schnedermann, J. Sollfrank, and U. W. Heinz, “Thermal phenomenology of hadrons from 200 AGeV S+S collisions”, *Phys. Rev. C* **48** (1993) 2462–2475, arXiv:9307020 [nucl-th].
- [94] ALICE Collaboration, B. Abelev *et al.*, “Centrality determination of Pb–Pb collisions at $\sqrt{s_{NN}} = 2.76$ TeV with ALICE”, *Phys. Rev. C* **88** (2013) 044909, arXiv:1301.4361 [nucl-ex].
- [95] ALICE Collaboration, K. Aamodt *et al.*, “The ALICE experiment at the CERN LHC”, *JINST* **3** (2008) S08002.
- [96] ALICE Collaboration, B. B. Abelev *et al.*, “Performance of the ALICE Experiment at the CERN LHC”, *Int. J. Mod. Phys. A* **29** (2014) 1430044, arXiv:1402.4476 [nucl-ex].
- [97] ALICE Collaboration, K. Aamodt *et al.*, “Alignment of the ALICE Inner Tracking System with cosmic-ray tracks”, *JINST* **5** (2010) P03003, arXiv:1001.0502 [physics.ins-det].

- [98] J. Alme *et al.*, “The ALICE TPC, a large 3-dimensional tracking device with fast readout for ultra-high multiplicity events”, *Nucl. Instrum. Meth. A* **622** (2010) 316–367, arXiv:1001.1950 [physics.ins-det].
- [99] A. Akindinov *et al.*, “Performance of the ALICE Time-Of-Flight detector at the LHC”, *Eur. Phys. J. Plus* **128** (2013) 44.
- [100] ALICE Collaboration, S. Acharya *et al.*, “The ALICE Transition Radiation Detector: construction, operation, and performance”, *Nucl. Instrum. Meth. A* **881** (2018) 88–127, arXiv:1709.02743 [physics.ins-det].
- [101] ALICE Collaboration, E. Abbas *et al.*, “Performance of the ALICE VZERO system”, *JINST* **8** (2013) P10016, arXiv:1306.3130 [nucl-ex].
- [102] W. Herr, “Beam-beam interactions”, <https://cds.cern.ch/record/941319>.
- [103] X.-N. Wang and M. Gyulassy, “HIJING: A Monte Carlo model for multiple jet production in pp, pA and AA collisions”, *Phys. Rev.* **D44** (1991) 3501–3516.
- [104] GEANT4 Collaboration, S. Agostinelli *et al.*, “GEANT4: A Simulation toolkit”, *Nucl. Instrum. Meth.* **A506** (2003) 250–303.
- [105] R. Barlow, “Systematic errors: Facts and fictions”, in *Advanced Statistical Techniques in Particle Physics.*, pp. 134–144. 2002. arXiv:hep-ex/0207026 [hep-ex]. <http://www.ippp.dur.ac.uk/Workshops/02/statistics/proceedings//barlow.pdf>.
- [106] ALICE Collaboration, S. Acharya *et al.*, “Production of charged pions, kaons, and (anti-)protons in Pb–Pb and inelastic pp collisions at $\sqrt{s_{NN}} = 5.02$ TeV”, *Phys. Rev. C* **101** (2020) 044907, arXiv:1910.07678 [nucl-ex].
- [107] V. M. Grichine, “A simple model for integral hadron-nucleus and nucleus-nucleus cross-sections”, *Nucl. Instrum. Meth. B* **267** (2009) 2460–2462.
- [108] V. Uzhinsky *et al.*, “Antinucleus-nucleus cross sections implemented in Geant4”, *Phys. Lett. B* **705** (2011) 235–239.
- [109] J. Allison *et al.*, “Recent developments in Geant4”, *Nucl. Instrum. Meth. A* **835** (2016) 186–225.
- [110] Q. Yan, V. Choutko, A. Oliva, and M. Paniccia, “Measurements of nuclear interaction cross sections with the Alpha Magnetic Spectrometer on the International Space Station”, *Nucl. Phys. A* **996** (2020) 121712.
- [111] ALICE Collaboration, B. Abelev *et al.*, “Centrality dependence of π , K, p production in Pb–Pb collisions at $\sqrt{s_{NN}} = 2.76$ TeV”, *Phys. Rev. C* **88** (2013) 044910, arXiv:1303.0737 [hep-ex].
- [112] A. Mazeliauskas, S. Floerchinger, E. Grossi, and D. Teaney, “Fast resonance decays in nuclear collisions”, *Eur. Phys. J. C* **79** (2019) 284, arXiv:1809.11049 [nucl-th].
- [113] A. Mazeliauskas, S. Floerchinger, E. Grossi, and D. Teaney, “FastReso–program for computing irreducible components of the particle distribution from direct resonance decays, GitHub repository”, <https://github.com/amazeliauskas/FastReso>. 2019.
- [114] A. Mazeliauskas and V. Vislavicius, “Temperature and fluid velocity on the freeze-out surface from π , K, p spectra in pp, p–Pb and Pb–Pb collisions”, *Phys. Rev. C* **101** (2020) 014910, arXiv:1907.11059 [hep-ph].















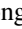




- [115] S. Grigoryan, “A three component model for hadron p_T -spectra in pp and Pb–Pb collisions at the LHC”, *Eur. Phys. J. A* **57** (2021) 328, arXiv:2109.07888 [hep-ph].
- [116] V. Vovchenko and H. Stoecker, “Thermal-FIST: A package for heavy-ion collisions and hadronic equation of state”, *Comput. Phys. Commun.* **244** (2019) 295–310, arXiv:1901.05249 [nucl-th].
- [117] **ALICE** Collaboration, S. Acharya *et al.*, “Production of (anti-) ^3He and (anti-) ^3H in p–Pb collisions at $\sqrt{s_{\text{NN}}} = 5.02$ TeV”, *Phys. Rev. C* **101** (2020) 044906, arXiv:1910.14401 [nucl-ex].
- [118] J. Steinheimer, calculation based on [68, 74], 2023.
- [119] K.-J. Sun, calculation based on [83, 84], 2023.

A The ALICE Collaboration

S. Acharya ¹²⁷, D. Adamová ⁸⁶, G. Aglieri Rinella ³³, M. Agnello ³⁰, N. Agrawal ⁵², Z. Ahammed ¹³⁵, S. Ahmad ¹⁶, S.U. Ahn ⁷², I. Ahuja ³⁸, A. Akhmedov ¹⁴¹, M. Al-Turany ⁹⁷, D. Aleksandrov ¹⁴¹, B. Alessandro ⁵⁷, H.M. Alfanda ⁶, R. Alfaro Molina ⁶⁸, B. Ali ¹⁶, A. Alici ²⁶, N. Alizadehvandchali ¹¹⁶, A. Alkin ³³, J. Alme ²¹, G. Alocco ⁵³, T. Alt ⁶⁵, A.R. Altamura ⁵¹, I. Altsybeev ⁹⁵, J.R. Alvarado ⁴⁵, M.N. Anaam ⁶, C. Andrei ⁴⁶, N. Andreou ¹¹⁵, A. Andronic ¹²⁶, E. Andronov ¹⁴¹, V. Anguelov ⁹⁴, F. Antinori ⁵⁵, P. Antonioli ⁵², N. Apadula ⁷⁴, L. Aphecetche ¹⁰³, H. Appelshäuser ⁶⁵, C. Arata ⁷³, S. Arcelli ²⁶, M. Aresti ²³, R. Arnaldi ⁵⁷, J.G.M.C.A. Arneiro ¹¹⁰, I.C. Arsene ²⁰, M. Arslandok ¹³⁸, A. Augustinus ³³, R. Averbeck ⁹⁷, M.D. Azmi ¹⁶, H. Baba ¹²⁴, A. Badalà ⁵⁴, J. Bae ¹⁰⁴, Y.W. Baek ⁴¹, X. Bai ¹²⁰, R. Bailhache ⁶⁵, Y. Bailung ⁴⁹, R. Bala ⁹¹, A. Balbino ³⁰, A. Baldisseri ¹³⁰, B. Balis ², D. Banerjee ⁴, Z. Banoo ⁹¹, F. Barile ³², L. Barioglio ⁹⁵, M. Barlou ⁷⁸, B. Barman ⁴², G.G. Barnaföldi ⁴⁷, L.S. Barnby ⁸⁵, E. Barreau ¹⁰³, V. Barret ¹²⁷, L. Barreto ¹¹⁰, C. Bartels ¹¹⁹, K. Barth ³³, E. Bartsch ⁶⁵, N. Bastid ¹²⁷, S. Basu ⁷⁵, G. Batigne ¹⁰³, D. Battistini ⁹⁵, B. Batyunya ¹⁴², D. Bauri ⁴⁸, J.L. Bazo Alba ¹⁰¹, I.G. Bearden ⁸³, C. Beattie ¹³⁸, P. Becht ⁹⁷, D. Behera ⁴⁹, I. Belikov ¹²⁹, A.D.C. Bell Hechavarria ¹²⁶, F. Bellini ²⁶, R. Bellwied ¹¹⁶, S. Belokurova ¹⁴¹, L.G.E. Beltran ¹⁰⁹, Y.A.V. Beltran ⁴⁵, G. Bencedi ⁴⁷, S. Beole ²⁵, Y. Berdnikov ¹⁴¹, A. Berdnikova ⁹⁴, L. Bergmann ⁹⁴, M.G. Besoiu ⁶⁴, L. Betev ³³, P.P. Bhaduri ¹³⁵, A. Bhasin ⁹¹, M.A. Bhat ⁴, B. Bhattacharjee ⁴², L. Bianchi ²⁵, N. Bianchi ⁵⁰, J. Bielčik ³⁶, J. Bielčiková ⁸⁶, A.P. Bigot ¹²⁹, A. Bilandzic ⁹⁵, G. Biro ⁴⁷, S. Biswas ⁴, N. Bize ¹⁰³, J.T. Blair ¹⁰⁸, D. Blau ¹⁴¹, M.B. Blidaru ⁹⁷, N. Bluhme ³⁹, C. Blume ⁶⁵, G. Boca ^{22,56}, F. Bock ⁸⁷, T. Bodova ²¹, S. Boi ²³, J. Bok ¹⁷, L. Boldizsár ⁴⁷, M. Bombara ³⁸, P.M. Bond ³³, G. Bonomi ^{134,56}, H. Borel ¹³⁰, A. Borissov ¹⁴¹, A.G. Borquez Carcamo ⁹⁴, H. Bossi ¹³⁸, E. Botta ²⁵, Y.E.M. Bouziani ⁶⁵, L. Bratrud ⁶⁵, P. Braun-Munzinger ⁹⁷, M. Bregant ¹¹⁰, M. Broz ³⁶, G.E. Bruno ^{96,32}, M.D. Buckland ²⁴, D. Budnikov ¹⁴¹, H. Buesching ⁶⁵, S. Bufalino ³⁰, P. Buhler ¹⁰², N. Burmasov ¹⁴¹, Z. Buthelezi ^{69,123}, A. Bylinkin ²¹, S.A. Bysiak ¹⁰⁷, J.C. Cabanillas Noris ¹⁰⁹, M. Cai ⁶, H. Caines ¹³⁸, A. Caliva ²⁹, E. Calvo Villar ¹⁰¹, J.M.M. Camacho ¹⁰⁹, P. Camerini ²⁴, F.D.M. Canedo ¹¹⁰, S.L. Cantway ¹³⁸, M. Carabas ¹¹³, A.A. Carballo ³³, F. Carnesecchi ³³, R. Caron ¹²⁸, L.A.D. Carvalho ¹¹⁰, J. Castillo Castellanos ¹³⁰, F. Catalano ^{33,25}, C. Ceballos Sanchez ¹⁴², I. Chakaberia ⁷⁴, P. Chakraborty ⁴⁸, S. Chandra ¹³⁵, S. Chapeland ³³, M. Chartier ¹¹⁹, S. Chattopadhyay ¹³⁵, S. Chattopadhyay ⁹⁹, T. Cheng ^{97,6}, C. Cheshkov ¹²⁸, B. Cheynis ¹²⁸, V. Chibante Barroso ³³, D.D. Chinellato ¹¹¹, E.S. Chizzali ^{11,95}, J. Cho ⁵⁹, S. Cho ⁵⁹, P. Chochula ³³, D. Choudhury ⁴², P. Christakoglou ⁸⁴, C.H. Christensen ⁸³, P. Christiansen ⁷⁵, T. Chujo ¹²⁵, M. Ciaccio ³⁰, C. Cicalo ⁵³, M.R. Ciupek ⁹⁷, G. Clai ^{III,52}, F. Colamaria ⁵¹, J.S. Colburn ¹⁰⁰, D. Colella ^{96,32}, M. Colocci ²⁶, M. Concas ^{IV,33}, G. Conesa Balbastre ⁷³, Z. Conesa del Valle ¹³¹, G. Contin ²⁴, J.G. Contreras ³⁶, M.L. Coquet ¹³⁰, P. Cortese ^{133,57}, M.R. Cosentino ¹¹², F. Costa ³³, S. Costanza ^{22,56}, C. Cot ¹³¹, J. Crkovská ⁹⁴, P. Crochet ¹²⁷, R. Cruz-Torres ⁷⁴, P. Cui ⁶, A. Dainese ⁵⁵, M.C. Danisch ⁹⁴, A. Danu ⁶⁴, P. Das ⁸⁰, P. Das ⁴, S. Das ⁴, A.R. Dash ¹²⁶, S. Dash ⁴⁸, A. De Caro ²⁹, G. de Cataldo ⁵¹, J. de Cuveland ³⁹, A. De Falco ²³, D. De Gruttola ²⁹, N. De Marco ⁵⁷, C. De Martin ²⁴, S. De Pasquale ²⁹, R. Deb ¹³⁴, R. Del Grande ⁹⁵, L. Dello Stritto ^{33,29}, W. Deng ⁶, P. Dhankher ¹⁹, D. Di Bari ³², A. Di Mauro ³³, B. Diab ¹³⁰, R.A. Diaz ^{142,7}, T. Dietel ¹¹⁴, Y. Ding ⁶, J. Ditzel ⁶⁵, R. Divià ³³, D.U. Dixit ¹⁹, Ø. Djuvsland ²¹, U. Dmitrieva ¹⁴¹, A. Dobrin ⁶⁴, B. Dönigus ⁶⁵, J.M. Dubinski ¹³⁶, A. Dubla ⁹⁷, S. Dudi ⁹⁰, P. Dupieux ¹²⁷, M. Durkac ¹⁰⁶, N. Dzalaiova ¹³, T.M. Eder ¹²⁶, R.J. Ehlers ⁷⁴, F. Eisenhut ⁶⁵, R. Ejima ⁹², D. Elia ⁵¹, B. Erazmus ¹⁰³, F. Ercolessi ²⁶, B. Espagnon ¹³¹, G. Eulisse ³³, D. Evans ¹⁰⁰, S. Evdokimov ¹⁴¹, L. Fabbietti ⁹⁵, M. Faggin ²⁸, J. Faivre ⁷³, F. Fan ⁶, W. Fan ⁷⁴, A. Fantoni ⁵⁰, M. Fasel ⁸⁷, A. Feliciello ⁵⁷, G. Feofilov ¹⁴¹, A. Fernández Téllez ⁴⁵, L. Ferrandi ¹¹⁰, M.B. Ferrer ³³, A. Ferrero ¹³⁰, C. Ferrero ⁵⁷, A. Ferretti ²⁵, V.J.G. Feuillard ⁹⁴, V. Filova ³⁶, D. Finogeev ¹⁴¹, F.M. Fionda ⁵³, E. Flatland ³³, F. Flor ¹¹⁶, A.N. Flores ¹⁰⁸, S. Foertsch ⁶⁹, I. Fokin ⁹⁴, S. Fokin ¹⁴¹, E. Fragiocomo ⁵⁸, E. Frajna ⁴⁷, U. Fuchs ³³, N. Funicello ²⁹, C. Furget ⁷³, A. Furs ¹⁴¹, T. Fusayasu ⁹⁸, J.J. Gaardhøje ⁸³, M. Gagliardi ²⁵, A.M. Gago ¹⁰¹, T. Gahlaut ¹⁰⁹, C.D. Galvan ¹⁰⁹, D.R. Gangadharan ¹¹⁶, P. Ganoti ⁷⁸, C. Garabatos ⁹⁷, A.T. Garcia ¹³¹, T. García Chávez ⁴⁵, E. Garcia-Solis ⁹, C. Gargiulo ³³, P. Gasik ⁹⁷, A. Gautam ¹¹⁸, M.B. Gay Ducati ⁶⁷, M. Germain ¹⁰³, A. Ghimouz ¹²⁵, C. Ghosh ¹³⁵, M. Giacalone ⁵², G. Gioachin ³⁰, P. Giubellino ^{97,57}, P. Giubilato ²⁸, A.M.C. Glaenger ¹³⁰, P. Gläsel ⁹⁴, E. Glimos ¹²², D.J.Q. Goh ⁷⁶, V. Gonzalez ¹³⁷, P. Gordeev ¹⁴¹, M. Gorgon ², K. Goswami ⁴⁹, S. Gotovac ³⁴, V. Grabski ⁶⁸, L.K. Graczykowski ¹³⁶, E. Grecka ⁸⁶, A. Grelli ⁶⁰, C. Grigoras ³³, V. Grigoriev ¹⁴¹, S. Grigoryan ^{142,1}, F. Grosa ³³, J.F. Grosse-Oetringhaus ³³, R. Grosso ⁹⁷, D. Grund ³⁶, N.A. Grunwald ⁹⁴, G.G. Guardianio ¹¹¹, R. Guernane ⁷³, M. Guilbaud ¹⁰³, K. Gulbrandsen ⁸³, T. Gündem ⁶⁵, T. Gunji ¹²⁴,

W. Guo⁶, A. Gupta⁹¹, R. Gupta⁹¹, R. Gupta⁴⁹, K. Gwizdziel¹³⁶, L. Gyulai⁴⁷, C. Hadjidakis¹³¹, F.U. Haider⁹¹, S. Haidlova³⁶, M. Haldar⁴, H. Hamagaki⁷⁶, A. Hamdi⁷⁴, Y. Han¹³⁹, B.G. Hanley¹³⁷, R. Hannigan¹⁰⁸, J. Hansen⁷⁵, J.W. Harris¹³⁸, A. Harton⁹, M.V. Hartung⁶⁵, H. Hassan¹¹⁷, D. Hatzifotiadou⁵², P. Hauer⁴³, L.B. Havener¹³⁸, E. Hellbär⁹⁷, H. Helstrup³⁵, M. Hemmer⁶⁵, T. Herman³⁶, G. Herrera Corral⁸, F. Herrmann¹²⁶, S. Herrmann¹²⁸, K.F. Hetland³⁵, B. Heybeck⁶⁵, H. Hillemanns³³, B. Hippolyte¹²⁹, F.W. Hoffmann⁷¹, B. Hofman⁶⁰, G.H. Hong¹³⁹, M. Horst⁹⁵, A. Horzyk², Y. Hou⁶, P. Hristov³³, C. Hughes¹²², P. Huhn⁶⁵, L.M. Huhta¹¹⁷, T.J. Humanic⁸⁸, A. Hutson¹¹⁶, D. Hutter³⁹, M.C. Hwang¹⁹, R. Ilkaev¹⁴¹, H. Ilyas¹⁴, M. Inaba¹²⁵, G.M. Innocenti³³, M. Ippolitov¹⁴¹, A. Isakov^{84,86}, T. Isidori¹¹⁸, M.S. Islam⁹⁹, M. Ivanov¹³, M. Ivanov⁹⁷, V. Ivanov¹⁴¹, K.E. Iversen⁷⁵, M. Jablonski², B. Jacak^{19,74}, N. Jacazio²⁶, P.M. Jacobs⁷⁴, S. Jadlovská¹⁰⁶, J. Jadlovsky¹⁰⁶, S. Jaelani⁸², C. Jahnke¹¹⁰, M.J. Jakubowska¹³⁶, M.A. Janik¹³⁶, T. Janson⁷¹, S. Ji¹⁷, S. Jia¹⁰, A.A.P. Jimenez⁶⁶, F. Jonas^{74,87,126}, D.M. Jones¹¹⁹, J.M. Jowett^{33,97}, J. Jung⁶⁵, M. Jung⁶⁵, A. Junique³³, A. Jusko¹⁰⁰, M.J. Kabus^{33,136}, J. Kaewjai¹⁰⁵, P. Kalinak⁶¹, A.S. Kalteyer⁹⁷, A. Kalweit³³, D. Karatovic⁸⁹, O. Karavichev¹⁴¹, T. Karavicheva¹⁴¹, P. Karczmarczyk¹³⁶, E. Karpechev¹⁴¹, U. Kebschull⁷¹, R. Keidel¹⁴⁰, D.L.D. Keijdener⁶⁰, M. Keil³³, B. Ketzer⁴³, S.S. Khade⁴⁹, A.M. Khan¹²⁰, S. Khan¹⁶, A. Khanzadeev¹⁴¹, Y. Kharlov¹⁴¹, A. Khatun¹¹⁸, A. Khuntia³⁶, Z. Khuranova⁶⁵, B. Kileng³⁵, B. Kim¹⁰⁴, C. Kim¹⁷, D.J. Kim¹¹⁷, E.J. Kim⁷⁰, J. Kim¹³⁹, J. Kim⁵⁹, J. Kim⁷⁰, M. Kim¹⁹, S. Kim¹⁸, T. Kim¹³⁹, K. Kimura⁹², S. Kirsch⁶⁵, I. Kisel³⁹, S. Kiselev¹⁴¹, A. Kisiel¹³⁶, J.P. Kitowski², J.L. Klay⁵, J. Klein³³, S. Klein⁷⁴, C. Klein-Bösing¹²⁶, M. Kleiner⁶⁵, T. Klemenz⁹⁵, A. Kluge³³, C. Kobdaj¹⁰⁵, T. Kollegger⁹⁷, A. Kondratyev¹⁴², N. Kondratyeva¹⁴¹, J. Konig⁶⁵, S.A. Konigstorfer⁹⁵, P.J. Konopka³³, G. Kornakov¹³⁶, M. Korwieser⁹⁵, S.D. Koryciak², A. Kotliarov⁸⁶, N. Kovacic⁸⁹, V. Kovalenko¹⁴¹, M. Kowalski¹⁰⁷, V. Kozuharov³⁷, I. Králik⁶¹, A. Kravčáková³⁸, L. Krcal^{33,39}, M. Krivda^{100,61}, F. Krizek⁸⁶, K. Krizkova Gajdosova³³, M. Kroesen⁹⁴, M. Krüger⁶⁵, D.M. Krupova³⁶, E. Kryshen¹⁴¹, V. Kučera⁵⁹, C. Kuhn¹²⁹, P.G. Kuijer⁸⁴, T. Kumaoka¹²⁵, D. Kumar¹³⁵, L. Kumar⁹⁰, N. Kumar⁹⁰, S. Kumar³², S. Kundu³³, P. Kurashvili⁷⁹, A. Kurepin¹⁴¹, A.B. Kurepin¹⁴¹, A. Kuryakin¹⁴¹, S. Kushpil⁸⁶, V. Kuskov¹⁴¹, M. Kutyla¹³⁶, M.J. Kweon⁵⁹, Y. Kwon¹³⁹, S.L. La Pointe³⁹, P. La Rocca²⁷, A. Lakrathok¹⁰⁵, M. Lamanna³³, A.R. Landou⁷³, R. Langoy¹²¹, P. Larionov³³, E. Laudi³³, L. Lautner^{33,95}, R. Lavicka¹⁰², R. Lea^{134,56}, H. Lee¹⁰⁴, I. Legrand⁴⁶, G. Legras¹²⁶, J. Lehrbach³⁹, T.M. Lelek², R.C. Lemmon⁸⁵, I. León Monzón¹⁰⁹, M.M. Lesch⁹⁵, E.D. Lesser¹⁹, P. Lévai⁴⁷, X. Li¹⁰, B.E. Liang-gilman¹⁹, J. Lien¹²¹, R. Lietava¹⁰⁰, I. Likmeta¹¹⁶, B. Lim²⁵, S.H. Lim¹⁷, V. Lindenstruth³⁹, A. Lindner⁴⁶, C. Lippmann⁹⁷, D.H. Liu⁶, J. Liu¹¹⁹, G.S.S. Liveraro¹¹¹, I.M. Lofnes²¹, C. Loizides⁸⁷, S. Lokos¹⁰⁷, J. Lomker⁶⁰, P. Loncar³⁴, X. Lopez¹²⁷, E. López Torres⁷, P. Lu^{97,120}, F.V. Lugo⁶⁸, J.R. Luhder¹²⁶, M. Lunardon²⁸, G. Luparello⁵⁸, Y.G. Ma⁴⁰, M. Mager³³, A. Maire¹²⁹, E.M. Majerz², M.V. Makariev³⁷, M. Malaev¹⁴¹, G. Malfattore²⁶, N.M. Malik⁹¹, Q.W. Malik²⁰, S.K. Malik⁹¹, L. Malinina^{I,VII,142}, D. Mallick^{131,80}, N. Mallick⁴⁹, G. Mandaglio^{31,54}, S.K. Mandal⁷⁹, V. Manko¹⁴¹, F. Manso¹²⁷, V. Manzari⁵¹, Y. Mao⁶, R.W. Marcjan², G.V. Margagliotti²⁴, A. Margotti⁵², A. Marín⁹⁷, C. Markert¹⁰⁸, P. Martinengo³³, M.I. Martínez⁴⁵, G. Martínez García¹⁰³, M.P.P. Martins¹¹⁰, S. Masciocchi⁹⁷, M. Masera²⁵, A. Masoni⁵³, L. Massacrier¹³¹, O. Massen⁶⁰, A. Mastroserio^{132,51}, O. Matonoha⁷⁵, S. Mattiazzo²⁸, A. Matyja¹⁰⁷, C. Mayer¹⁰⁷, A.L. Mazuecos³³, F. Mazzaschi²⁵, M. Mazzilli³³, J.E. Mdhuli¹²³, Y. Melikyan⁴⁴, A. Menchaca-Rocha⁶⁸, J.E.M. Mendez⁶⁶, E. Meninno¹⁰², A.S. Menon¹¹⁶, M. Meres¹³, Y. Miake¹²⁵, L. Micheletti³³, D.L. Mihaylov⁹⁵, K. Mikhaylov^{142,141}, D. Miśkowiec⁹⁷, A. Modak⁴, B. Mohanty⁸⁰, M. Mohisin Khan^{V,16}, M.A. Molander⁴⁴, S. Monira¹³⁶, C. Mordasini¹¹⁷, D.A. Moreira De Godoy¹²⁶, I. Morozov¹⁴¹, A. Morsch³³, T. Mrnjavac³³, V. Muccifora⁵⁰, S. Muhuri¹³⁵, J.D. Mulligan⁷⁴, A. Mulliri²³, M.G. Munhoz¹¹⁰, R.H. Munzer⁶⁵, H. Murakami¹²⁴, S. Murray¹¹⁴, L. Musa³³, J. Musinsky⁶¹, J.W. Myrcha¹³⁶, B. Naik¹²³, A.I. Nambrath¹⁹, B.K. Nandi⁴⁸, R. Nania⁵², E. Nappi⁵¹, A.F. Nassirpour¹⁸, A. Nath⁹⁴, C. Nattrass¹²², M.N. Naydenov³⁷, A. Neagu²⁰, A. Negru¹¹³, E. Nekrasova¹⁴¹, L. Nellen⁶⁶, R. Nepeivoda⁷⁵, S. Nese²⁰, G. Neskovic³⁹, N. Nicassio⁵¹, B.S. Nielsen⁸³, E.G. Nielsen⁸³, S. Nikolaev¹⁴¹, S. Nikulin¹⁴¹, V. Nikulin¹⁴¹, F. Noferini⁵², S. Noh¹², P. Nomokonov¹⁴², J. Norman¹¹⁹, N. Novitzky⁸⁷, P. Nowakowski¹³⁶, A. Nyanin¹⁴¹, J. Nystrand²¹, S. Oh¹⁸, A. Ohlson⁷⁵, V.A. Okorokov¹⁴¹, J. Oleniacz¹³⁶, A. Onnerstad¹¹⁷, C. Oppedisano⁵⁷, A. Ortiz Velasquez⁶⁶, J. Otwinowski¹⁰⁷, M. Oya⁹², K. Oyama⁷⁶, Y. Pachmayer⁹⁴, S. Padhan⁴⁸, D. Pagano^{134,56}, G. Paic⁶⁶, S. Paisano-Guzmán⁴⁵, A. Palasciano⁵¹, S. Panebianco¹³⁰, H. Park¹²⁵, H. Park¹⁰⁴, J. Park⁵⁹, J.E. Parkkila³³, Y. Patley⁴⁸, B. Paul²³, M.M.D.M. Paulino¹¹⁰,

H. Pei⁶, T. Peitzmann⁶⁰, X. Peng¹¹, M. Pennisi²⁵, S. Perciballi²⁵, D. Peresunko¹⁴¹, G.M. Perez⁷,
 Y. Pestov¹⁴¹, V. Petrov¹⁴¹, M. Petrovici⁴⁶, R.P. Pezzi^{103,67}, S. Piano⁵⁸, M. Pikna¹³, P. Pillot¹⁰³,
 O. Pinazza^{52,33}, L. Pinsky¹¹⁶, C. Pinto⁹⁵, S. Pisano⁵⁰, M. Płoskoń⁷⁴, M. Planinic⁸⁹, F. Pliquett⁶⁵,
 M.G. Poghosyan⁸⁷, B. Polichtchouk¹⁴¹, S. Politano³⁰, N. Poljak⁸⁹, A. Pop⁴⁶,
 S. Porteboeuf-Houssais¹²⁷, V. Pozdniakov¹⁴², I.Y. Pozos⁴⁵, K.K. Pradhan⁴⁹, S.K. Prasad⁴,
 S. Prasad⁴⁹, R. Preghenella⁵², F. Prino⁵⁷, C.A. Pruneau¹³⁷, I. Pshenichnov¹⁴¹, M. Puccio³³,
 S. Pucillo²⁵, Z. Pugelova¹⁰⁶, S. Qiu⁸⁴, L. Quaglia²⁵, S. Ragoni¹⁵, A. Rai¹³⁸,
 A. Rakotozafindrabe¹³⁰, L. Ramello^{133,57}, F. Rami¹²⁹, T.A. Rancien⁷³, M. Rasa²⁷, S.S. Räsänen⁴⁴,
 R. Rath⁵², M.P. Rauch²¹, I. Ravasenga³³, K.F. Read^{87,122}, C. Reckziegel¹¹², A.R. Redelbach³⁹,
 K. Redlich^{VI,79}, C.A. Reetz⁹⁷, H.D. Regules-Medel⁴⁵, A. Rehman²¹, F. Reidt³³, H.A. Reme-Ness³⁵,
 Z. Rescakova³⁸, K. Reygers⁹⁴, A. Riabov¹⁴¹, V. Riabov¹⁴¹, R. Ricci²⁹, M. Richter²⁰,
 A.A. Riedel⁹⁵, W. Riegler³³, A.G. Riffero²⁵, C. Ristea⁶⁴, M.V. Rodriguez³³, M. Rodríguez
 Cahuantzi⁴⁵, S.A. Rodríguez Ramírez⁴⁵, K. Røed²⁰, R. Rogalev¹⁴¹, E. Rogochaya¹⁴²,
 T.S. Rogoschinski⁶⁵, D. Rohr³³, D. Röhrich²¹, P.F. Rojas⁴⁵, S. Rojas Torres³⁶, P.S. Rokita¹³⁶,
 G. Romanenko²⁶, F. Ronchetti⁵⁰, A. Rosano^{31,54}, E.D. Rosas⁶⁶, K. Roslon¹³⁶, A. Rossi⁵⁵,
 A. Roy⁴⁹, S. Roy⁴⁸, N. Rubini²⁶, D. Ruggiano¹³⁶, R. Rui²⁴, P.G. Russek², R. Russo⁸⁴,
 A. Rustamov⁸¹, E. Ryabinkin¹⁴¹, Y. Ryabov¹⁴¹, A. Rybicki¹⁰⁷, H. Rytönen¹¹⁷, J. Ryu¹⁷,
 W. Rzesza¹³⁶, O.A.M. Saariimaki⁴⁴, S. Sadhu³², S. Sadosky¹⁴¹, J. Saetre²¹, K. Šafařík³⁶, P. Saha⁴²,
 S.K. Saha⁴, S. Saha⁸⁰, B. Sahoo⁴⁸, B. Sahoo⁴⁹, R. Sahoo⁴⁹, S. Sahoo⁶², D. Sahu⁴⁹, P.K. Sahu⁶²,
 J. Saini¹³⁵, K. Sajdakova³⁸, S. Sakai¹²⁵, M.P. Salvan⁹⁷, S. Sambyal⁹¹, D. Samitz¹⁰², I. Sanna^{33,95},
 T.B. Saramela¹¹⁰, D. Sarkar⁸³, P. Sarma⁴², V. Sarritzu²³, V.M. Sarti⁹⁵, M.H.P. Sas³³, S. Sawan⁸⁰,
 E. Scapparone⁵², J. Schambach⁸⁷, H.S. Scheid⁶⁵, C. Schiaua⁴⁶, R. Schicker⁹⁴, F. Schlepfer⁹⁴,
 A. Schmah⁹⁷, C. Schmidt⁹⁷, H.R. Schmidt⁹³, M.O. Schmidt³³, M. Schmidt⁹³, N.V. Schmidt⁸⁷,
 A.R. Schmier¹²², R. Schotter¹²⁹, A. Schröter³⁹, J. Schukraft³³, K. Schweda⁹⁷, G. Scioli²⁶,
 E. Scomparin⁵⁷, J.E. Seger¹⁵, Y. Sekiguchi¹²⁴, D. Sekihata¹²⁴, M. Selina⁸⁴, I. Selyuzhenkov⁹⁷,
 S. Senyukov¹²⁹, J.J. Seo⁹⁴, D. Serebryakov¹⁴¹, L. Serkin⁶⁶, L. Šerkšnytė⁹⁵, A. Sevcenco⁶⁴,
 T.J. Shaba⁶⁹, A. Shabetai¹⁰³, R. Shahoyan³³, A. Shangaraev¹⁴¹, B. Sharma⁹¹, D. Sharma⁴⁸,
 H. Sharma⁵⁵, M. Sharma⁹¹, S. Sharma⁷⁶, S. Sharma⁹¹, U. Sharma⁹¹, A. Shatat¹³¹, O. Sheibani¹¹⁶,
 K. Shigaki⁹², M. Shimomura⁷⁷, J. Shin¹², S. Shirinkin¹⁴¹, Q. Shou⁴⁰, Y. Sibiriak¹⁴¹, S. Siddhanta⁵³,
 T. Siemiarczuk⁷⁹, T.F. Silva¹¹⁰, D. Silvermyr⁷⁵, T. Simantathammakul¹⁰⁵, R. Simeonov³⁷, B. Singh⁹¹,
 B. Singh⁹⁵, K. Singh⁴⁹, R. Singh⁸⁰, R. Singh⁹¹, R. Singh⁴⁹, S. Singh¹⁶, V.K. Singh¹³⁵,
 V. Singhal¹³⁵, T. Sinha⁹⁹, B. Sitar¹³, M. Sitta^{133,57}, T.B. Skaali²⁰, G. Skorodumovs⁹⁴,
 M. Slupecki⁴⁴, N. Smirnov¹³⁸, R.J.M. Snellings⁶⁰, E.H. Solheim²⁰, J. Song¹⁷, C. Sonnabend^{33,97},
 J.M. Sonneveld⁸⁴, F. Soramel²⁸, A.B. Soto-herandez⁸⁸, R. Spijkers⁸⁴, I. Sputowska¹⁰⁷, J. Staa⁷⁵,
 J. Stachel⁹⁴, I. Stan⁶⁴, P.J. Steffanic¹²², S.F. Stiefelmaier⁹⁴, D. Stocco¹⁰³, I. Storehaug²⁰,
 P. Stratmann¹²⁶, S. Strazzi²⁶, A. Sturmiolo^{31,54}, C.P. Stylianidis⁸⁴, A.A.P. Suaide¹¹⁰, C. Suire¹³¹,
 M. Sukhanov¹⁴¹, M. Suljic³³, R. Sultanov¹⁴¹, V. Sumberia⁹¹, S. Sumowidagdo⁸², I. Szarka¹³,
 M. Szymkowski¹³⁶, S.F. Taghavi⁹⁵, G. Taillepied⁹⁷, J. Takahashi¹¹¹, G.J. Tambave⁸⁰, S. Tang⁶,
 Z. Tang¹²⁰, J.D. Tapia Takaki¹¹⁸, N. Tapus¹¹³, L.A. Tarasovicova¹²⁶, M.G. Tarzila⁴⁶, G.F. Tassielli³²,
 A. Tauro³³, G. Tejeda Muñoz⁴⁵, A. Telesca³³, L. Terlizzi²⁵, C. Terrevoli¹¹⁶, S. Thakur⁴,
 D. Thomas¹⁰⁸, A. Tikhonov¹⁴¹, N. Tiltmann¹²⁶, A.R. Timmins¹¹⁶, M. Tkacik¹⁰⁶, T. Tkacik¹⁰⁶,
 A. Toia⁶⁵, R. Tokumoto⁹², K. Tomohiro⁹², N. Topilskaya¹⁴¹, M. Toppi⁵⁰, T. Tork¹³¹, P.V. Torres⁶⁶,
 V.V. Torres¹⁰³, A.G. Torres Ramos³², A. Trifiro^{31,54}, A.S. Triolo^{33,31,54}, S. Tripathy⁵²,
 T. Tripathy⁴⁸, S. Trogolo³³, V. Trubnikov³, W.H. Trzaska¹¹⁷, T.P. Trzcinski¹³⁶, A. Tumkin¹⁴¹,
 R. Turrisi⁵⁵, T.S. Tveter²⁰, K. Ullaland²¹, B. Ulukutlu⁹⁵, A. Uras¹²⁸, M. Urioni¹³⁴, G.L. Usai²³,
 M. Vala³⁸, N. Valle²², L.V.R. van Doremalen⁶⁰, M. van Leeuwen⁸⁴, C.A. van Veen⁹⁴, R.J.G. van
 Weelden⁸⁴, P. Vande Vyvre³³, D. Varga⁴⁷, Z. Varga⁴⁷, M. Vasileiou⁷⁸, A. Vasiliev¹⁴¹, O. Vázquez
 Doce⁵⁰, O. Vazquez Rueda¹¹⁶, V. Vechernin¹⁴¹, E. Vercellin²⁵, S. Vergara Limón⁴⁵, R. Verma⁴⁸,
 L. Vermunt⁹⁷, R. Vértesi⁴⁷, M. Verweij⁶⁰, L. Vickovic³⁴, Z. Vilakazi¹²³, O. Villalobos Baillie¹⁰⁰,
 A. Villani²⁴, A. Vinogradov¹⁴¹, T. Virgili²⁹, M.M.O. Virta¹¹⁷, V. Vislavicius⁷⁵, A. Vodopyanov¹⁴²,
 B. Volkel³³, M.A. Völkl⁹⁴, S.A. Voloshin¹³⁷, G. Volpe³², B. von Haller³³, I. Vorobyev³³,
 N. Vozniuk¹⁴¹, J. Vrláková³⁸, J. Wan⁴⁰, C. Wang⁴⁰, D. Wang⁴⁰, Y. Wang⁴⁰, Y. Wang⁶,
 A. Wegrzynek³³, F.T. Weiglhofer³⁹, S.C. Wenzel³³, J.P. Wessels¹²⁶, J. Wiechula⁶⁵, J. Wikne²⁰,
 G. Wilk⁷⁹, J. Wilkinson⁹⁷, G.A. Willems¹²⁶, B. Windelband⁹⁴, M. Winn¹³⁰, J.R. Wright¹⁰⁸,
 W. Wu⁴⁰, Y. Wu¹²⁰, R. Xu⁶, A. Yadav⁴³, A.K. Yadav¹³⁵, Y. Yamaguchi⁹², S. Yang²¹, S. Yano⁹²,
 E.R. Yeats¹⁹, Z. Yin⁶, I.-K. Yoo¹⁷, J.H. Yoon⁵⁹, H. Yu¹², S. Yuan²¹, A. Yuncu⁹⁴, V. Zaccolo²⁴,

C. Zampolli ³³, F. Zanone ⁹⁴, N. Zardoshti ³³, A. Zarochentsev ¹⁴¹, P. Závada ⁶³, N. Zaviyalov¹⁴¹, M. Zhalov ¹⁴¹, B. Zhang ⁶, C. Zhang ¹³⁰, L. Zhang ⁴⁰, S. Zhang ⁴⁰, X. Zhang ⁶, Y. Zhang¹²⁰, Z. Zhang ⁶, M. Zhao ¹⁰, V. Zhrebchevskii ¹⁴¹, Y. Zhi¹⁰, C. Zhong⁴⁰, D. Zhou ⁶, Y. Zhou ⁸³, J. Zhu ^{55,6}, Y. Zhu⁶, S.C. Zugravel ⁵⁷, N. Zurlo ^{134,56}

Affiliation Notes

^I Deceased

^{II} Also at: Max-Planck-Institut für Physik, Munich, Germany

^{III} Also at: Italian National Agency for New Technologies, Energy and Sustainable Economic Development (ENEA), Bologna, Italy

^{IV} Also at: Dipartimento DET del Politecnico di Torino, Turin, Italy

^V Also at: Department of Applied Physics, Aligarh Muslim University, Aligarh, India

^{VI} Also at: Institute of Theoretical Physics, University of Wrocław, Poland

^{VII} Also at: An institution covered by a cooperation agreement with CERN

Collaboration Institutes

¹ A.I. Alikhanyan National Science Laboratory (Yerevan Physics Institute) Foundation, Yerevan, Armenia

² AGH University of Krakow, Cracow, Poland

³ Bogolyubov Institute for Theoretical Physics, National Academy of Sciences of Ukraine, Kiev, Ukraine

⁴ Bose Institute, Department of Physics and Centre for Astroparticle Physics and Space Science (CAPSS), Kolkata, India

⁵ California Polytechnic State University, San Luis Obispo, California, United States

⁶ Central China Normal University, Wuhan, China

⁷ Centro de Aplicaciones Tecnológicas y Desarrollo Nuclear (CEADEN), Havana, Cuba

⁸ Centro de Investigación y de Estudios Avanzados (CINVESTAV), Mexico City and Mérida, Mexico

⁹ Chicago State University, Chicago, Illinois, United States

¹⁰ China Institute of Atomic Energy, Beijing, China

¹¹ China University of Geosciences, Wuhan, China

¹² Chungbuk National University, Cheongju, Republic of Korea

¹³ Comenius University Bratislava, Faculty of Mathematics, Physics and Informatics, Bratislava, Slovak Republic

¹⁴ COMSATS University Islamabad, Islamabad, Pakistan

¹⁵ Creighton University, Omaha, Nebraska, United States

¹⁶ Department of Physics, Aligarh Muslim University, Aligarh, India

¹⁷ Department of Physics, Pusan National University, Pusan, Republic of Korea

¹⁸ Department of Physics, Sejong University, Seoul, Republic of Korea

¹⁹ Department of Physics, University of California, Berkeley, California, United States

²⁰ Department of Physics, University of Oslo, Oslo, Norway

²¹ Department of Physics and Technology, University of Bergen, Bergen, Norway

²² Dipartimento di Fisica, Università di Pavia, Pavia, Italy

²³ Dipartimento di Fisica dell'Università and Sezione INFN, Cagliari, Italy

²⁴ Dipartimento di Fisica dell'Università and Sezione INFN, Trieste, Italy

²⁵ Dipartimento di Fisica dell'Università and Sezione INFN, Turin, Italy

²⁶ Dipartimento di Fisica e Astronomia dell'Università and Sezione INFN, Bologna, Italy

²⁷ Dipartimento di Fisica e Astronomia dell'Università and Sezione INFN, Catania, Italy

²⁸ Dipartimento di Fisica e Astronomia dell'Università and Sezione INFN, Padova, Italy

²⁹ Dipartimento di Fisica 'E.R. Caianiello' dell'Università and Gruppo Collegato INFN, Salerno, Italy

³⁰ Dipartimento DISAT del Politecnico and Sezione INFN, Turin, Italy

³¹ Dipartimento di Scienze MIFT, Università di Messina, Messina, Italy

³² Dipartimento Interateneo di Fisica 'M. Merlin' and Sezione INFN, Bari, Italy

³³ European Organization for Nuclear Research (CERN), Geneva, Switzerland

³⁴ Faculty of Electrical Engineering, Mechanical Engineering and Naval Architecture, University of Split, Split, Croatia

³⁵ Faculty of Engineering and Science, Western Norway University of Applied Sciences, Bergen, Norway

- ³⁶ Faculty of Nuclear Sciences and Physical Engineering, Czech Technical University in Prague, Prague, Czech Republic
- ³⁷ Faculty of Physics, Sofia University, Sofia, Bulgaria
- ³⁸ Faculty of Science, P.J. Šafárik University, Košice, Slovak Republic
- ³⁹ Frankfurt Institute for Advanced Studies, Johann Wolfgang Goethe-Universität Frankfurt, Frankfurt, Germany
- ⁴⁰ Fudan University, Shanghai, China
- ⁴¹ Gangneung-Wonju National University, Gangneung, Republic of Korea
- ⁴² Gauhati University, Department of Physics, Guwahati, India
- ⁴³ Helmholtz-Institut für Strahlen- und Kernphysik, Rheinische Friedrich-Wilhelms-Universität Bonn, Bonn, Germany
- ⁴⁴ Helsinki Institute of Physics (HIP), Helsinki, Finland
- ⁴⁵ High Energy Physics Group, Universidad Autónoma de Puebla, Puebla, Mexico
- ⁴⁶ Horia Hulubei National Institute of Physics and Nuclear Engineering, Bucharest, Romania
- ⁴⁷ HUN-REN Wigner Research Centre for Physics, Budapest, Hungary
- ⁴⁸ Indian Institute of Technology Bombay (IIT), Mumbai, India
- ⁴⁹ Indian Institute of Technology Indore, Indore, India
- ⁵⁰ INFN, Laboratori Nazionali di Frascati, Frascati, Italy
- ⁵¹ INFN, Sezione di Bari, Bari, Italy
- ⁵² INFN, Sezione di Bologna, Bologna, Italy
- ⁵³ INFN, Sezione di Cagliari, Cagliari, Italy
- ⁵⁴ INFN, Sezione di Catania, Catania, Italy
- ⁵⁵ INFN, Sezione di Padova, Padova, Italy
- ⁵⁶ INFN, Sezione di Pavia, Pavia, Italy
- ⁵⁷ INFN, Sezione di Torino, Turin, Italy
- ⁵⁸ INFN, Sezione di Trieste, Trieste, Italy
- ⁵⁹ Inha University, Incheon, Republic of Korea
- ⁶⁰ Institute for Gravitational and Subatomic Physics (GRASP), Utrecht University/Nikhef, Utrecht, Netherlands
- ⁶¹ Institute of Experimental Physics, Slovak Academy of Sciences, Košice, Slovak Republic
- ⁶² Institute of Physics, Homi Bhabha National Institute, Bhubaneswar, India
- ⁶³ Institute of Physics of the Czech Academy of Sciences, Prague, Czech Republic
- ⁶⁴ Institute of Space Science (ISS), Bucharest, Romania
- ⁶⁵ Institut für Kernphysik, Johann Wolfgang Goethe-Universität Frankfurt, Frankfurt, Germany
- ⁶⁶ Instituto de Ciencias Nucleares, Universidad Nacional Autónoma de México, Mexico City, Mexico
- ⁶⁷ Instituto de Física, Universidade Federal do Rio Grande do Sul (UFRGS), Porto Alegre, Brazil
- ⁶⁸ Instituto de Física, Universidad Nacional Autónoma de México, Mexico City, Mexico
- ⁶⁹ iThemba LABS, National Research Foundation, Somerset West, South Africa
- ⁷⁰ Jeonbuk National University, Jeonju, Republic of Korea
- ⁷¹ Johann-Wolfgang-Goethe Universität Frankfurt Institut für Informatik, Fachbereich Informatik und Mathematik, Frankfurt, Germany
- ⁷² Korea Institute of Science and Technology Information, Daejeon, Republic of Korea
- ⁷³ Laboratoire de Physique Subatomique et de Cosmologie, Université Grenoble-Alpes, CNRS-IN2P3, Grenoble, France
- ⁷⁴ Lawrence Berkeley National Laboratory, Berkeley, California, United States
- ⁷⁵ Lund University Department of Physics, Division of Particle Physics, Lund, Sweden
- ⁷⁶ Nagasaki Institute of Applied Science, Nagasaki, Japan
- ⁷⁷ Nara Women's University (NWU), Nara, Japan
- ⁷⁸ National and Kapodistrian University of Athens, School of Science, Department of Physics, Athens, Greece
- ⁷⁹ National Centre for Nuclear Research, Warsaw, Poland
- ⁸⁰ National Institute of Science Education and Research, Homi Bhabha National Institute, Jatni, India
- ⁸¹ National Nuclear Research Center, Baku, Azerbaijan
- ⁸² National Research and Innovation Agency - BRIN, Jakarta, Indonesia
- ⁸³ Niels Bohr Institute, University of Copenhagen, Copenhagen, Denmark
- ⁸⁴ Nikhef, National institute for subatomic physics, Amsterdam, Netherlands
- ⁸⁵ Nuclear Physics Group, STFC Daresbury Laboratory, Daresbury, United Kingdom
- ⁸⁶ Nuclear Physics Institute of the Czech Academy of Sciences, Husinec-Řež, Czech Republic
- ⁸⁷ Oak Ridge National Laboratory, Oak Ridge, Tennessee, United States

- ⁸⁸ Ohio State University, Columbus, Ohio, United States
⁸⁹ Physics department, Faculty of science, University of Zagreb, Zagreb, Croatia
⁹⁰ Physics Department, Panjab University, Chandigarh, India
⁹¹ Physics Department, University of Jammu, Jammu, India
⁹² Physics Program and International Institute for Sustainability with Knotted Chiral Meta Matter (SKCM2), Hiroshima University, Hiroshima, Japan
⁹³ Physikalisches Institut, Eberhard-Karls-Universität Tübingen, Tübingen, Germany
⁹⁴ Physikalisches Institut, Ruprecht-Karls-Universität Heidelberg, Heidelberg, Germany
⁹⁵ Physik Department, Technische Universität München, Munich, Germany
⁹⁶ Politecnico di Bari and Sezione INFN, Bari, Italy
⁹⁷ Research Division and ExtreMe Matter Institute EMMI, GSI Helmholtzzentrum für Schwerionenforschung GmbH, Darmstadt, Germany
⁹⁸ Saga University, Saga, Japan
⁹⁹ Saha Institute of Nuclear Physics, Homi Bhabha National Institute, Kolkata, India
¹⁰⁰ School of Physics and Astronomy, University of Birmingham, Birmingham, United Kingdom
¹⁰¹ Sección Física, Departamento de Ciencias, Pontificia Universidad Católica del Perú, Lima, Peru
¹⁰² Stefan Meyer Institut für Subatomare Physik (SMI), Vienna, Austria
¹⁰³ SUBATECH, IMT Atlantique, Nantes Université, CNRS-IN2P3, Nantes, France
¹⁰⁴ Sungkyunkwan University, Suwon City, Republic of Korea
¹⁰⁵ Suranaree University of Technology, Nakhon Ratchasima, Thailand
¹⁰⁶ Technical University of Košice, Košice, Slovak Republic
¹⁰⁷ The Henryk Niewodniczanski Institute of Nuclear Physics, Polish Academy of Sciences, Cracow, Poland
¹⁰⁸ The University of Texas at Austin, Austin, Texas, United States
¹⁰⁹ Universidad Autónoma de Sinaloa, Culiacán, Mexico
¹¹⁰ Universidade de São Paulo (USP), São Paulo, Brazil
¹¹¹ Universidade Estadual de Campinas (UNICAMP), Campinas, Brazil
¹¹² Universidade Federal do ABC, Santo Andre, Brazil
¹¹³ Universitatea Nationala de Stiinta si Tehnologie Politehnica Bucuresti, Bucharest, Romania
¹¹⁴ University of Cape Town, Cape Town, South Africa
¹¹⁵ University of Derby, Derby, United Kingdom
¹¹⁶ University of Houston, Houston, Texas, United States
¹¹⁷ University of Jyväskylä, Jyväskylä, Finland
¹¹⁸ University of Kansas, Lawrence, Kansas, United States
¹¹⁹ University of Liverpool, Liverpool, United Kingdom
¹²⁰ University of Science and Technology of China, Hefei, China
¹²¹ University of South-Eastern Norway, Kongsberg, Norway
¹²² University of Tennessee, Knoxville, Tennessee, United States
¹²³ University of the Witwatersrand, Johannesburg, South Africa
¹²⁴ University of Tokyo, Tokyo, Japan
¹²⁵ University of Tsukuba, Tsukuba, Japan
¹²⁶ Universität Münster, Institut für Kernphysik, Münster, Germany
¹²⁷ Université Clermont Auvergne, CNRS/IN2P3, LPC, Clermont-Ferrand, France
¹²⁸ Université de Lyon, CNRS/IN2P3, Institut de Physique des 2 Infinis de Lyon, Lyon, France
¹²⁹ Université de Strasbourg, CNRS, IPHC UMR 7178, F-67000 Strasbourg, France, Strasbourg, France
¹³⁰ Université Paris-Saclay, Centre d’Etudes de Saclay (CEA), IRFU, Département de Physique Nucléaire (DPhN), Saclay, France
¹³¹ Université Paris-Saclay, CNRS/IN2P3, IJCLab, Orsay, France
¹³² Università degli Studi di Foggia, Foggia, Italy
¹³³ Università del Piemonte Orientale, Vercelli, Italy
¹³⁴ Università di Brescia, Brescia, Italy
¹³⁵ Variable Energy Cyclotron Centre, Homi Bhabha National Institute, Kolkata, India
¹³⁶ Warsaw University of Technology, Warsaw, Poland
¹³⁷ Wayne State University, Detroit, Michigan, United States
¹³⁸ Yale University, New Haven, Connecticut, United States
¹³⁹ Yonsei University, Seoul, Republic of Korea
¹⁴⁰ Zentrum für Technologie und Transfer (ZTT), Worms, Germany

¹⁴¹ Affiliated with an institute covered by a cooperation agreement with CERN

¹⁴² Affiliated with an international laboratory covered by a cooperation agreement with CERN.